

Inferring Inference

Rajkumar Vasudeva Raju^{1,2,*}, Zhe Li², Scott Linderman³, and Xaq Pitkow^{1,2,3,4,5,6,*}

¹Department of ECE, Rice University

²Department of Neuroscience, Baylor College of Medicine

³Department of Statistics, Stanford University

⁴Neuroscience Institute, Carnegie Mellon University

⁵Department of Machine Learning, Carnegie Mellon University

⁶Center for Neuroscience and Artificial Intelligence, Baylor College of Medicine

*Corresponding authors

ABSTRACT

Patterns of microcircuitry in the cerebral cortex suggest that the brain has an array of repeated elementary or “canonical” computational units. However, neural representations are distributed, so the relevant computations may only be related indirectly to single-neuron transformations. It thus remains an open challenge how to define canonical *distributed* computations. Here we integrate normative and algorithmic theories of neural computation to present a mathematical framework for inferring canonical distributed computations from large-scale neural activity patterns. At the normative level, we hypothesize that the brain creates a structured internal model of its environment, positing latent causes that explain its sensory inputs, and using those sensory inputs to infer the states of the latent causes. At the algorithmic level, we propose that this inference process is a nonlinear message-passing algorithm on a graph-structured model of the world. Given a time series of neural activity during a perceptual inference task, our analysis framework simultaneously finds (*i*) the neural representation of the relevant latent variables, (*ii*) interactions between these latent variables that define the brain’s internal model of the world, and (*iii*) message-functions that specify the inference algorithm. Crucially, to be identifiable, this message-passing algorithm must use canonical nonlinear computations shared across the graph. With enough data, these targeted computational properties are then statistically distinguishable due to the symmetries inherent in any canonical computation, up to a joint global transformation of all interactions and the message-passing functions. As a concrete demonstration of this framework, we analyze artificial neural recordings generated by a model brain that implicitly implements an approximate inference algorithm on a probabilistic graphical model. Given external inputs and noisy neural activity from the model brain, we successfully recover the latent variables, their neural representation and dynamics, and canonical message-functions that govern the dynamics. Finally, analysis of these models reveals features of experimental design required to successfully extract canonical computations from neural data. Overall, this framework provides a new tool for discovering interpretable structure in complex neural recordings.

1 Introduction

We hypothesize that emergent computations in the brain are lawful and obey compressible rules: lawful, because there are a few canonical nonlinear operations, repeated in some form across many inputs or conditions, that govern its computations; and compressible because those operations can be summarized with far fewer parameters than needed to describe arbitrary dynamics. More specifically, we assume these computations define a dynamic message-passing algorithm for probabilistic inference, as we will describe below. We also assume that this dynamical structure is hidden in the collective action of many neurons. In this paper we develop a conceptual framework for discovering this hidden message-passing algorithm within large-scale measurements of neural activity, and we demonstrate a first application of this framework to a simulated brain to infer its inference algorithm.

Message-passing is an algorithm that reduces complex, often intractable global computations over many related variables into a sequence of simpler local operations. For example, Google’s PageRank is a well-known message-passing algorithm that estimates the importance of web pages by distributing and recombining estimates of web page values along web links. Generally, message-passing algorithms work by iteratively sending information, or messages, along edges in a graph relating those variables. A *canonical* computation is a fundamental computation that repeats across brain regions and modalities to apply the same operations in a variety of contexts [1, 2, 3]. Because message-passing algorithms use the same operations for all edges on a graph, they are an instance of canonical computation. Although message-passing can be used for any graph-structured computation, we are particularly interested in probabilistic inference on a graph-structured world.

Consider two levels of canonical computations: (i) the neural circuit/implementation level and (ii) the algorithmic/representational level [4]. In a sense, a vanilla recurrent neural network is one simple example of a message-passing algorithm with canonical operations at the circuit level, where the neural activities are the variables, their connections form the graph, and the neural nonlinear activation functions are the canonical operations. Canonical computations at that circuit level could include feedforward inhibition, divisive normalization, coincidence detection, gating information between different cortical areas, and working memory storage [2, 3]. In contrast, here we propose that other canonical computations emerge only at the algorithmic level, hidden in population dynamics. These distributed canonical computations could even be more interpretable and perceptually relevant than local canonical mechanisms.

To discover such computations, our work integrates normative, algorithmic, and mechanistic theories [4] of recurrent nonlinear processing in the brain. We develop structured statistical models for fitting neural data and revealing these distributed computational motifs, and we demonstrate how to connect these theories to the mechanistic level. Figure 1 is a schematic of our framework, showing the relationship between the mechanistic model (Figure 1A) and the algorithmic model (Figure 1B–D). Sections below introduce the mathematical formalism behind the schematic’s components.

At the normative level, we hypothesize that the brain has an internal model of the world, positing latent variables that explain its sensory data. The Good Regulator Theorem states that the best way to control the world is to have a good model of the world [5] and, conversely, the No Free Lunch Theorems [6] show that no algorithm can be superior to any other over all possible tasks or stimulus ensembles. Whether from extensive training, inherited innate knowledge, or a combination of the two [7], one expects a sufficiently flexible intelligent system will successfully create an internal model that parallels the relevant structure of its natural environment, specifically by representing a set of sparsely interacting latent causes [8]. One natural manifestation of this general framework is a Bayesian brain [9, 10] that represents complex probability distributions using a formalism called probabilistic graphical models: these models use graphs to describe conditional independence relationships between latent variables [11, 12], and algorithms can exploit these graphs for efficient approximate inference.

At the algorithmic level, we propose that inference in the brain is implemented by nonlinear dynamics describing the flow of statistical information through that graph-structured internal model of the world [13, 14]. Specifically, we hypothesize that these dynamics are structured as message-passing on its internal model of the world that the brain uses to synthesize its sensory evidence and choose actions.

At the mechanistic level, and to connect this message-passing algorithm to data, we need to specify how neural activity represents the latent variables and how computations will be implemented through neural dynamics. The neuron doctrine states that a neuron is the basic anatomical and physiological unit of the nervous system. This has been the central tenet driving neuroscience research in the past century. In contrast, it has also become clear that neural representations are highly distributed [15, 16, 17, 18]. Even though the physical causes of computations are biological neurons, we argue that distributed processing is a better level for understanding the hypothesized message-passing.

There are two distinct senses in which a neural code could be distributed: information about a single variable could be distributed across many neurons (a population code [19]), and single neurons could contain information about many variables (mixed selectivity [20]). Both properties are thought to coexist in the brain. This makes it harder to understand structured processing. It would be much easier to understand if the brain dedicated distinct populations purely to distinct variables [21, 22]. Although localist codes have long assumed such dedicated modular architectures [23, 24], ample evidence shows that task-relevant representations are not always localized [15, 25]. When structured computation does not directly parallel structured anatomy, new methods are needed to extract and describe these computational structures [26].

Our work provides a conceptual approach to interpret how the collective dynamics of neuronal populations are structured to perform behaviorally relevant computations via message-passing. To make this approach concrete, we also introduce some simplifications and demonstrate in practice that we can recover the algorithm of a simulated brain.

2 Results

2.1 Message-passing as a model for inference in the brain

To discover the brain’s computations, we assume that relevant canonical operations are shared across an entire unknown graph of unknown interacting variables, and we infer latent states, their coupling, and how they evolve over time. Although this framework is technically agnostic about the meaning of these neural responses, we are motivated by the hypothesis that the brain performs approximate Bayesian inference, and therefore we apply this framework to inference in a structured probabilistic graphical model [11]. First we will describe the underlying canonical dynamics at an abstract level; second we consider latent representations of probabilistic graphical models. We then combine these two

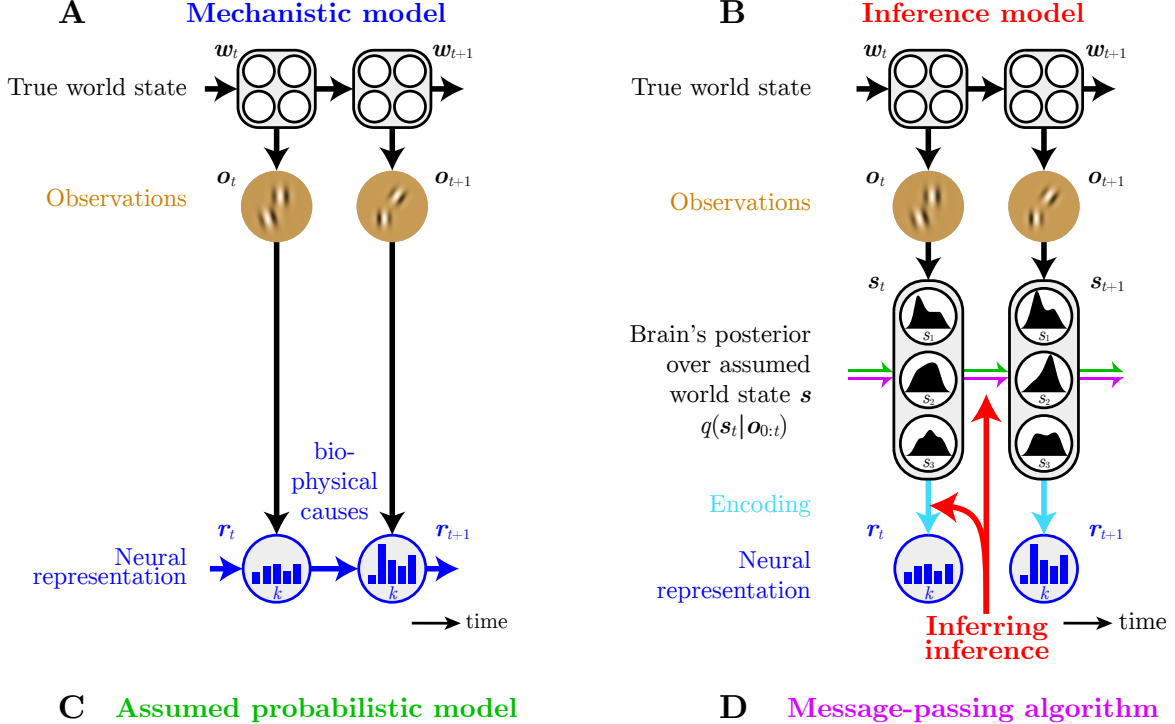


Figure 1: **Schematic of inferring inference.** **A:** Mechanistic model has observations \mathbf{o}_t at time t generated from an evolving world state \mathbf{w}_t . These observations affect the intrinsic dynamics of neural responses \mathbf{r}_t . **B:** We impose a low-dimensional normative interpretation upon these mechanistic dynamics, where the reduced dimensions encode approximate posterior probabilities over assumed task-relevant variables \mathbf{s} , which may differ from the true world state \mathbf{w} . **C:** The dynamics are structured according to a sparsely connected probabilistic graphical model, where signals propagate through task-relevant dimensions only along edges in the underlying graph. **D:** This propagation is assumed to be lawful, following a canonical nonlinear message function \mathcal{M} that is shared by all edges, but is modulated by coupling strengths that are specific to each edge.

ingredients to demonstrate how to identify the latent variable representation and the corresponding population-level message-passing computations.

2.1.1 Message-passing by canonical computations

We use the general structure of a ‘graph neural network’ (GNN) [27, 28, 29] to describe the dynamics of a generic message-passing algorithm. In a graph neural network, each node in an undirected graph \mathcal{G} is associated with a vector-valued state \mathbf{x}_i for node i , and a vector-valued parameter \mathbf{J}_{ij} for each edge (i, j) . On every time step, each node sends a *message* to each of its neighboring nodes. The message $\mathbf{m}_{j \rightarrow i, t+1}$ from node j to i at time step $t+1$ depends on the state of the source and destination nodes as well as on their edge parameter:

$$\mathbf{m}_{j \rightarrow i, t+1} = \mathcal{M}(\mathbf{x}_{jt}, \mathbf{x}_{it}, \mathbf{J}_{ij}) \quad (1)$$

where \mathcal{M} is the message function. Next, an aggregation function \mathcal{A} combines incoming messages into a single message for the destination node:

$$\mathbf{M}_{i,t+1} = \mathcal{A}(\{\mathbf{m}_{j \rightarrow i, t+1} ; j \in \text{Nei}_i\}) \quad (2)$$

where Nei_i is the set of all neighbors of node i in \mathcal{G} . Aggregation functions are typically permutation-invariant, *i.e.* they depend only on the set of incoming messages, and not on which node they come from (although these messages themselves do depend on the source nodes and edge parameters). Example aggregation functions include a simple sum, mean, or product. Finally, every node updates its state based on its previous state, any current external inputs \mathbf{v}_{it} to that node, and the aggregated message:

$$\mathbf{x}_{i,t+1} = \mathcal{U}(\mathbf{x}_{it}, \mathbf{v}_{it}, \mathbf{M}_{i,t+1}) \quad (3)$$

where \mathcal{U} is the node update function, and \mathbf{v}_{it} is the external input at node i at time t . Since the nodes' transitions to next states $\mathbf{x}_{i,t+1}$ depend collectively on the past only through the current states \mathbf{x}_t , these message-passing dynamics are Markovian.

An important property of these dynamics is that the message-update, aggregation, and node-update functions each have the same form at all locations on the graph. The specific messages vary with context, and the message function depends on edge parameters which may differ between edges, but all messages have the *same* dependence on edge parameters. This imposes a canonical organization at the algorithmic level, or what we could call an algorithmic symmetry.

2.1.2 Probabilistic Graphical Models (PGMs)

Having described the core computational dynamics underlying our framework, we now turn to an additional motivating hypothesis about what the message-passing might be computing. Aligned with the rich history of the Bayesian brain hypothesis, we assume that the brain uses a mental model of the world to unconsciously perform probabilistic inference [9, 10]. We elaborate on this general idea by assuming that the brain structures its mental model as a probabilistic graphical model (PGM) [30, 11, 31, 32, 14, 33]. PGMs elegantly specify structured relationships between variables that matter in tasks, using a graph to specify conditional dependencies. Mathematically, we use PGMs to represent probability distributions $p(\mathbf{s})$ over a vector of latent variables \mathbf{s} . Usually the relevant probabilities are also conditioned on some observations \mathbf{o} , yielding the posterior distribution $p(\mathbf{s}|\mathbf{o})$.

For simplicity, this paper concentrates on pairwise undirected graphical models. (In the Discussion we address generalizations to dynamic, directed, causal graphs with higher-order interactions.) A pairwise undirected PGM \mathcal{G} uses nodes \mathcal{V} and edges \mathcal{E} to represent a probability distribution $p(\mathbf{s}|\mathbf{o})$. Each node i represents one variable s_i . These variables interact with each other along edges (i, j) that indicate conditional dependencies. The joint distribution is described by the Boltzmann distribution $p(\mathbf{s}|\mathbf{o}) \propto e^{-E(\mathbf{s}|\mathbf{o})}$ with an energy $E(\mathbf{s}|\mathbf{o})$ that decomposes into a sum of simpler terms, one for each node and edge. Critically, where there is no edge, the energy of interactions is zero, and the corresponding variables are conditionally independent given all other variables. This graph structure imposes restrictions that allow us to represent many complex multivariate distributions in terms of simpler structure.

Natural tasks usually involve only a subset of all variables, or perhaps even a single variable s_i . Thus, an intelligent agent benefits from computing the marginal probability $p_i(s_i|\mathbf{o})$ of that variable. That marginal probability can then be used to select good actions. Marginalization is therefore a central inference problem that brains face, and serves as a concrete example of a canonical computational problem. However, in general, marginalization is intractable, requiring the integration over all variables except the relevant one. Instead of performing an intractable computation by brute force, the brain may approximate these computations, leading to approximate posterior marginals $q_i(s_i|\mathbf{o})$ instead of the true ones.

2.1.3 Message-passing for probabilistic graphical models

We would like to understand the computational dynamics leading to q_i . Our motivating theory assumes that the brain uses message-passing for approximate marginalization to obtain probabilities of individual latent variables. Message-passing can exploit the graph structure of the probabilistic graphical model to perform these important approximate inference computations efficiently [34, 35, 36].

We can establish a natural correspondence between the structure of a PGM and the structure of a graph neural network [34, 36]. In a probabilistic graphical model, each node corresponds to a variable s_i . In a graph neural network, each node contains a hidden state vector \mathbf{x}_i that represents the information relevant to that node. One can construct the network so that as the message-passing computations evolve, this state vector \mathbf{x}_i comes to parameterize a target distribution, $q_i(s_i|\mathbf{x}_i) \approx q_i(s_i|\mathbf{o})$ [34, 36]. Many distinct inference algorithms — such as mean-field inference [37], belief propagation [38], expectation propagation [39], and others — all arise from different nonlinear transformations, characterized by the choice of functions in a message-passing algorithm. Even Gibbs sampling can be viewed as a message-passing algorithm with a stochastic update.

Biological nonlinear canonical functions in the brain might conceivably implement even smarter variants that are well-suited to the natural environment [14]. Our goal is to identify the canonical functions that define the brain’s inference algorithms.

2.1.4 Neural manifestations of latent dynamics

At the mechanistic level, information processing is implemented by the collective behavior of neural populations. Consistent with established properties of neural codes, in which information is distributed across redundant neurons with mixed selectivity [20, 40], we expect that the brain’s internal model of the world, which specifies latent variables and their interactions, is not directly reflected in the activity or connections of individual neurons. Rather, it is *implicit* in the mechanistic interactions between overlapping neural populations. Thus, it is crucial to quantify how information is represented and transformed in a low-dimensional latent space that is embedded in high-dimensional neural responses.

We assume that population activity r encodes the underlying message-passing model in a potentially complicated and nonlinear fashion, described as $r_t = \mathcal{R}(\mathbf{x}_t, \eta_t)$, where \mathcal{R} is the neural encoding function, \mathbf{x}_t is the state of all nodes at time t , and η_t is noise or variability unrelated to the mental model. (In our example application we will assume a simple linear encoding, but later we discuss generalizations to nonlinear encodings.) Here we assume that the spatial pattern of neural activity instantaneously (within some modest time window of perhaps 100ms) represents the information about \mathbf{x}_t , although we could also consider alternative models in which probabilities are represented through temporal patterns [41, 42, 43] or spatiotemporal patterns [44]. In a spatial code for probability, the population activity r_t evolves in time such that the dynamics of the encoded node states \mathbf{x}_t conforms to the update equations 1-3, thereby implicitly representing the dynamics of message-passing inference on the underlying graphical model [13, 14].

Our *Neural Message-Passing hypothesis* is that brain computations satisfy these assumptions: the brain approximates probabilistic inference on a generative model of the world using nonlinear message-passing between overlapping neuronal populations.

2.2 Framework for Inferring Inference

To reveal the brain’s inferential computations under this assumed structure, we develop an analysis framework that can identify a latent graphical model and message-passing dynamics from stochastic neural data and sensory inputs. We call this framework *Inferring Inference*. If our hypothesized structure is correct, then we expect that a model fit by the inferring inference framework will recover a nonlinear message-passing algorithm accurately enough to predict neural population responses to novel stimuli.

Given input stimuli/sensory observations and neural measurements from a perceptual inference task, our aim is to simultaneously find (i) the neural encoding of relevant latent variables, (ii) interactions between these variables that define the brain’s probabilistic model of the world, and (iii) the canonical message functions that specify the implicit inference algorithm. In order to do this, we construct a Hidden Markov Model (HMM) in which each of these elements affects the likelihood for the measured neural activity given the sensory observations; inferring the above elements now reduces to a maximum likelihood estimation problem.

Suppose that we are given sensory observations \mathbf{o}_t and the recorded neural population activity r_t . The sensory observations are generated from an evolving true world latent state \mathbf{w}_t . The neural activity evolves directly in response to these sensory inputs as depicted in the mechanistic model in Fig. 1A. Our normative interpretation of these mechanistic dynamics, depicted in Fig. 1B, is that the neural activity encodes approximate posterior probabilities over *assumed* task-relevant variables \mathbf{s} . (Note that the brain’s latent model variables \mathbf{s} can differ from the true causal variables in the world \mathbf{w} .) We denote the brain’s posterior over its assumed world state \mathbf{s} by $q(\mathbf{s}_t | \mathbf{o}_{0:t})$, which we assume is structured according to a probabilistic graphical model (PGM) that is unknown to us (Fig. 1C).

Since real-world tasks often depend on individual variables, not on the full joint distribution of all variables, we assume that the brain’s algorithm uses the graph structure to infer approximate marginal posteriors q_i for each node i in its graphical model. We denote the brain’s parameterization of those posteriors by dynamic node states \mathbf{x}_{it} .¹

We model the latent dynamics of \mathbf{x}_t by the generic message-passing algorithm specified by equations 1 – 3. Note that now there are actually two different types of dynamic latent variables: first, the causal variables in the world, whether true world states \mathbf{w} or those according to the brain’s internal model \mathbf{s} , are latent variables from the perspective of the brain; and second, the node states \mathbf{x} that define the brain’s algorithm are latent variables for us from our perspective

¹For simplicity, we assume that the brain assumes the world and observations are both static, so according to the brain all its latent dynamics are merely a consequence of its own algorithmic dynamics. This leads to the brain drawing incorrect inferences when the observations and/or underlying states are actually dynamic. In the Discussion we address extensions for inferences that account for world dynamics.

	<i>Symbol</i>	<i>Meaning</i>
World model	w	true world state
	s	brain's assumed latent world state
	o	sensory observation
	$q(\cdot)$	approximate posterior over assumed world state
	x	parameter of posterior
	t	time
Neural message-passing	\mathcal{G}	graph of interactions between assumed latents
	x_{it}	vector-valued posterior parameter of node i at time t
	J_{ij}	vector-valued model parameter of edge (i, j)
	v_{it}	local input at node i at time t
	$m_{j \rightarrow i, t}$	message from node j to i at time t
	\mathcal{M}	message function
	\mathcal{A}	message aggregation function
	\mathcal{U}	node update function
	\mathcal{R}	neural encoding function
TAP model	s_i	latent variable corresponding to node i
	J_{ij}	direct statistical interaction between nodes i and j
	o_t	external input at time t
	V	coupling matrix between input and latent variables
	x_{it}	approximate marginal posterior probability of s_i at time t
	\mathbf{x}_t	vector of marginal probabilities at time t
	R	neural encoding matrix
Model fitting	r_t	population neural activity at time t
	$p(\cdot)$	probability of data under message-passing model
	G	canonical message-passing parameters
	G_{abc}	coefficient of the polynomial term $J_{ij}^a x_{it}^b x_{jt}^c$
	θ	vector of all parameters to be estimated (R, V, J, G)

Table 1: Glossary of notation.

as scientists. We parameterize the coupling between each interacting pair of variables as J_{ij} . The mapping from the latent node states x_{it} to the population neural activity r_t is specified by the encoding function \mathcal{R} . We collect all of the parameters into one big vector θ , whose components include parameters of the neural encoding function, the coupling parameters, and the message-passing functions. We estimate the parameters that best explain the measured neural responses to those sensory observations by maximum likelihood, using the Markov dynamics of message-passing to make the computation tractable (Methods).

In the next section we apply this general framework to simulated neural data whose latent dynamics accord with the neural message passing hypothesis, and evaluate our ability to recover the ground truth as a function of various experimental properties.

2.3 A concrete model brain implicitly performing approximate inference

As a concrete demonstration of our framework, we apply our method to artificial neural recordings generated by a model brain. We construct a brain that implicitly implements an advanced mean-field inference on a binary world state, following the Thouless-Anderson-Palmer (TAP) equation [45] derived originally to describe disordered physical systems and subsequently used in a variety of applications [46, 47, 48]. This example is a non-trivial instance of a hidden message-passing algorithm for approximate inference.

At a *normative* level, this inference model estimates marginal probabilities of N_s binary latent variables, $s \in \{-1, 1\}^{N_s}$, from the joint distribution $q(s|o) \propto \exp(s^\top J s + s^\top V o)$. Here o are the sensory inputs, V is a linear mapping from

these inputs to the latent space, and J is a coupling matrix that defines the graphical model, with $J_{ij} = 0$ for states s_i and s_j that do not interact directly.

At the *algorithmic* level, the latent state \mathbf{x} represents the approximate marginal probability. For the TAP equation, each assumed world state s_i is just one binary variable, so we can summarize each marginal distribution compactly by just a single number, $x_i = q_i(s_i = +1|\mathbf{o})$, which specifies the approximate probability that the latent state is +1. We chose the TAP model because it has nontrivial canonical nonlinear dynamics yet with a relatively simple low-order polynomial form (Methods 4.1.1).

At the *mechanistic* level, the model brain that enacts this implicit inference algorithm is a two-layer recurrent neural network (RNN) with ReLU activations. We train the RNN such that the target low-dimensional latent dynamics are approximately linearly embedded by a matrix R into the neural activity: $\mathbf{r}_t \approx R\mathbf{x}_t + \eta_t$ where η_t is additive white Gaussian noise (see Methods 4.1.2). Thus, by construction, this simulated brain implicitly implements inference by message-passing on the underlying graphical model (Fig. 2).

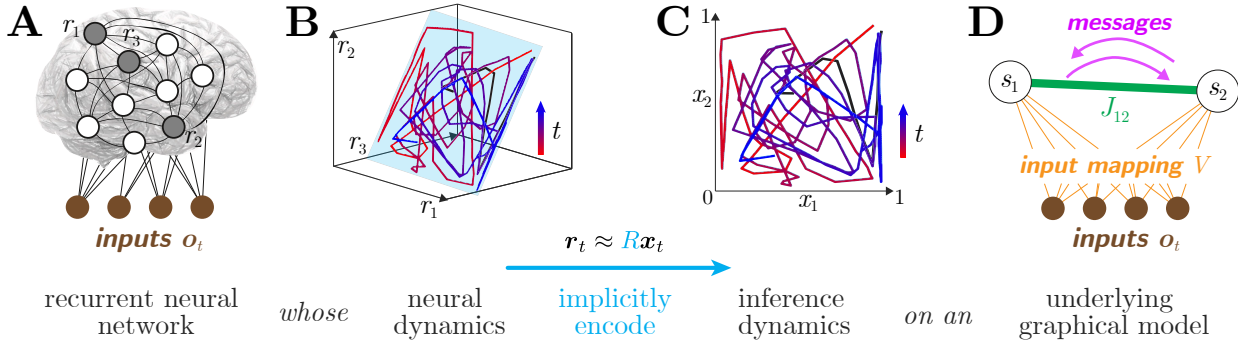


Figure 2: **A model brain**, implemented as a trained RNN (a), has neuronal dynamics (b) that are an approximate linear embedding of the TAP inference dynamics (c) on a binary probabilistic graphical model (d). In this illustration, the joint activity of the three gray neurons traces out a trajectory (time indicated as red to blue) in a 2D subspace corresponding to the inference dynamics of two interacting variables.

2.4 Inferring the model brain's inference algorithm

To infer the inference of this model brain, whose algorithm we pretend we don't know, we make the following simplifying assumptions: (i) the neural activity is known to be a linear embedding of the latent dynamics, (ii) the aggregation and node-update functions are known, and (iii) the process noise ξ_t and the encoding noise η_t are Gaussian-distributed with known covariances. We express the unknown message-function in a low-order polynomial basis as

$$\mathcal{M}(x_i, x_j, J_{ij}) = \sum_{a,b,c} G_{abc} J_{ij}^a x_i^b x_j^c \quad (4)$$

where the indices $0 \leq a, b, c \leq 2$ are integer powers of monomial terms with corresponding coefficients G_{abc} . These coefficients G , which we call the canonical message-parameters, are global (common to all parts of the graphical model) and specify the nonlinearity of the message-function. The non-zero coefficients that specify the true message-function in the TAP equation (equation 6) are: $G_{101} = 2$, $G_{201} = 4$, $G_{202} = -4$, $G_{211} = -8$ and $G_{212} = 8$.

Given inputs \mathbf{o}_t and measurements \mathbf{r}_t from the model brain, our goal is to recover the latent dynamics. This requires us to simultaneously estimate the parameters $\theta = (R, V, J, G)$ containing the linear embedding matrix R , linear mapping from inputs to the latent space V , the coupling matrix J that defines the graphical model, and the canonical message-parameters G .

To infer these latent dynamics we use the Expectation-Maximization (EM) algorithm [49]. However, the E step requires us to compute the posterior distribution of the latent variables, a challenging inference problem in models with nonlinear latent dynamics. Here we used a particle filter [50, 51], also known as Sequential Monte Carlo (SMC), to flexibly approximate the posterior over latent states as a point cloud of sampled state trajectories \mathbf{x}_t . This iterative combination of particle filters with EM for estimating unknown parameters in latent variable models is known as Particle EM [50]. We apply this approach to measurements from the TAP brain to obtain the maximum likelihood estimate of its parameters $\hat{\theta}$ (details in Methods 4.2.1).

2.5 Inferring inference in an example TAP brain

Consider an example TAP brain with $N_r = 500$ neurons that receives inputs of dimension $N_o = 10$ and encodes $N_s = 10$ latent variables. The coupling matrix J is a randomly generated sparse symmetric matrix, shown as a graphical model in Fig. 3D. The neural encoding matrix R and the input mapping matrix V are also randomly generated, and both distribute their respective signals densely across all neurons. Random input signals o_t evoked neural responses r_t . Here we allow the measurement of all 500 neurons in the model brain, but we expect that if there were more neurons then they would be largely redundant with the ones we do measure, reflecting the same latent dynamics but with a higher signal to noise ratio [52].

Given this model brain, we would now like to infer its parameters using only the measured neural activity and sensory inputs. Right away we are faced with the problem that we don't know in advance the number of latent variables encoded by the brain. We thus apply the Particle EM algorithm multiple times with different numbers m of latent variables, find the most likely parameters, and choose the value of m with the highest likelihood averaged over multiple batches of test data. This procedure reliably identifies the correct number of latent variables (Figure 3E).

Once the number of latent variables has been identified, we can examine the inference solution with the highest likelihood. Fig. 3F and G compare the model fit and the ground truth, for both neural measurements and the latent dynamics using previously unseen test inputs. The red and blue data points correspond to our initial and final estimates of parameters. After Particle EM converges, these estimated parameters reliably recover the ground truth latent dynamics. Figure 3H,I shows that our method recovers accurate estimates of both the neural encoding matrix \hat{R} and the input mapping \hat{V} matrix.

Note, however, that the inferred coupling matrix \hat{J} and message passing parameters \hat{G} differ from their true value, even though the model provides an excellent fit to the observable data. This is a consequence of the degeneracies in our parameterization [53]. To break these degeneracies, we perform a greedy backward optimization, progressively pruning G to find a sparse subset of message-passing parameters that best explain the latent dynamics (Methods 4.2.2). Fig. 3J–L shows that after this refinement step, the inferred message-passing parameters and the couplings closely match the ground truth. The small discrepancy that remains in 3J reflects a degeneracy that our regularization cannot resolve. Notice that this discrepancy does not appreciably affect the inference, since the latent variables are nonetheless inferred correctly (3G). With suitable regularization, we are thus able to infer the implicit inference computations of our model brain.

2.6 Better experimental design for better inferences

An important factor for the success of our analysis framework is experimental design, *i.e.* choosing stimuli or tasks that can reveal the relevant encoding and nonlinear dynamics. Strong stimuli may drive latent variables to extremes of their range, which makes it easier to identify the dimensions that encode these variables. However, these same stimuli may be so strong that they overwhelm the effects of recurrent interactions, which makes it difficult to learn these interactions. Conversely, weak stimuli may bring a network to an approximately linear regime where the interactions are discernible but it is hard to differentiate between relevant latent dimensions. Moreover, weak stimuli may not expose the interesting nonlinear interactions that distinguish different computational algorithms. We found that it is best to present a distribution of stimuli with a wide range of intensities. This allows us to identify both the embedding and the dynamics.

We illustrate this in the context of our model brain as follows. Since EM converges to local optima, the choice of initialization for the parameters is critical. The initial value for the embedding matrix is important for resolving the encoding degeneracy. Our latent variables correspond to marginal probabilities of binary variables, and thus all lie between 0 and 1. The latent dynamics therefore often exhibit highly non-Gaussian distributions. We obtain an initial estimate of the neural embedding \hat{R} using Independent Component Analysis (ICA) [54] on measured neural activity, since ICA is particularly well-suited to discovering non-Gaussian dimensions. The quality of this estimate, however, depends on the strength of the input signal relative to the coupling strengths. To control the input strength, our experimental stimuli use an amplitude scaling factor \tilde{g}_o to quantify the relative input gain (see Methods 4.1.3 for details).

Fig. 4 show how the ground truth latent activity, initial estimate of the neural embedding, and the Particle EM estimates each vary as a function of this gain for the example TAP brain in Fig. 3. In the case of low gain inputs (Fig. 4, top), the weak constraints result in ICA estimates that have large deviations from the ground truth. Extremely high gain inputs are not ideal either (Fig. 4, bottom). In this condition, the latent activity is biased towards maximal or minimal values, and we observe that ICA fails to recover a good estimate of the encoding matrix \hat{R} along multiple dimensions. When \tilde{g}_o is in the range [20, 25], we observe that the latent dynamics explore their full range, resulting in a fairly uniform

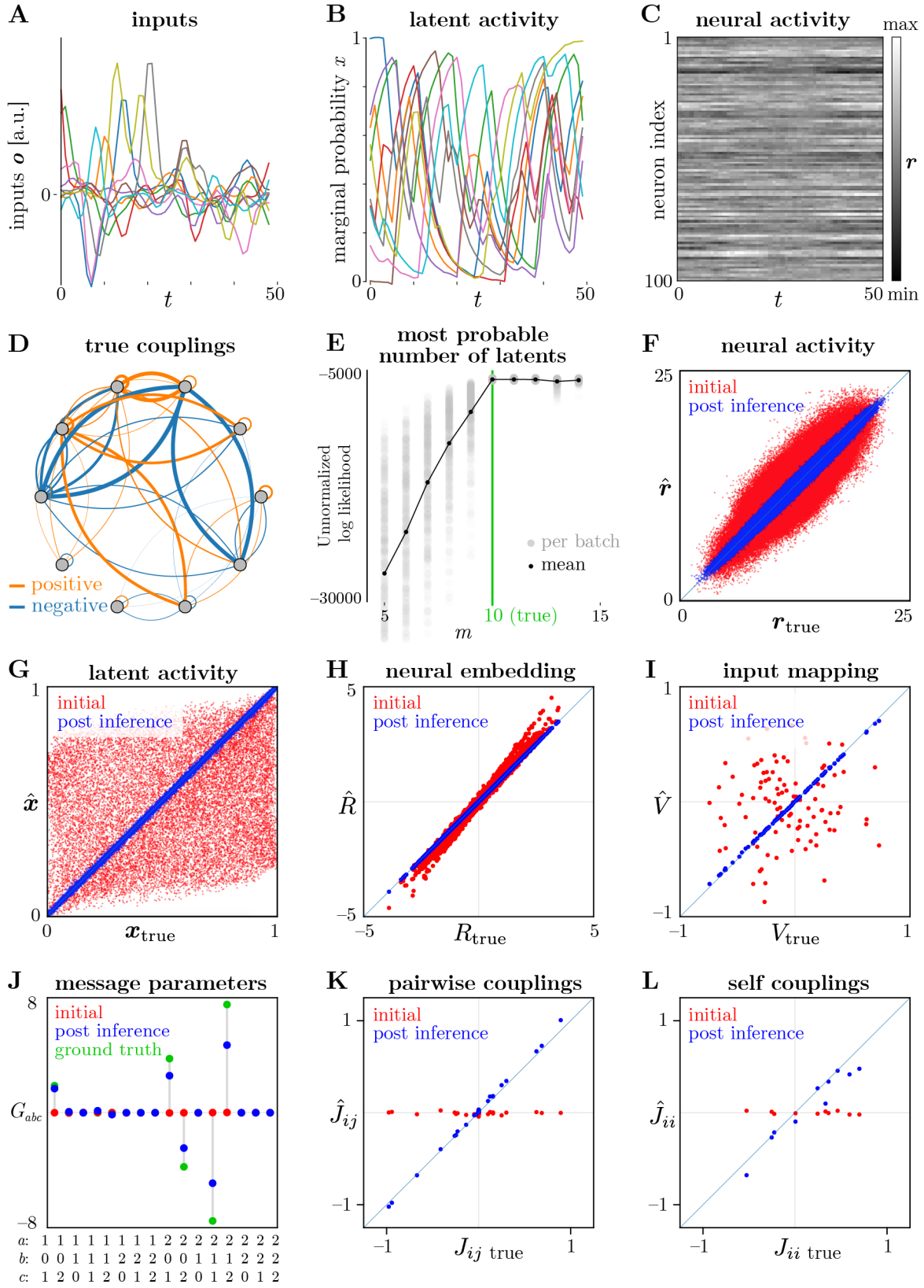


Figure 3: (Caption on next page.)

Figure 3: **Inferring inference in an example TAP brain.** The example brain has $N_r = 500$ neurons that encode the dynamics of $N_s = 10$ latent variables. We use Particle EM to fit the neural measurements and successfully recover the latent dynamics, followed by a backward greedy optimization to refine the estimates of the message parameters \hat{G} and the coupling matrix \hat{J} . **A:** Dynamic inputs \mathbf{o} to the model, used by the simulated brain to infer states of the external world. **B:** The internal model’s latent states \mathbf{x} are the approximate marginal probabilities q of each world state according to the internal model. **C:** These latent states are encoded in the distributed activity \mathbf{r} of neurons. **D:** The ground truth graphical model, where the edges correspond to couplings. Positive and negative couplings are colored orange and blue, respectively, and the edge thickness represents the relative magnitude. **E:** Observed data log-likelihood at the end of Particle EM vs. the assumed number of latent variables. The likelihood is highest for the true number of latents, ($\hat{N}_s = 10$, green line). **F:** Scatter plot of the fit to neural activity vs. the ground truth. **G:** Scatter plot of the inferred latent activity vs. the ground truth. In panels **F** and **G**, each data point corresponds to one time sample of one neuron/latent variable. The red and blue data correspond to the initial and post-inference values, respectively. **H** and **I:** Scatter plot of the estimates vs. ground truth values of the elements of the neural embedding and input mapping matrices, respectively. **J:** The true (green), initial (red), and final estimates (green) values of the canonical message parameters G_{abc} . **K** and **L:** Scatter plot of the estimates vs. ground truth values of the pairwise coupling and self-coupling (diagonal) terms of J .

distribution of the latent states over time. Under this condition, ICA is able to obtain a reliable neural embedding \hat{R} (middle row, third column). With this initial estimate, the Particle EM algorithm is biased towards the correct subspace for the latent dynamics (Fig. 4: middle row, fourth and fifth columns from the left in Fig. 4). For the inference results with the example TAP brain in Fig. 3, we used a broad range of input strengths $\tilde{g}_0 \sim [5, 25]$ to enable the model brain to exhibit a wide repertoire of its dynamics, and this enabled us to recover the true internal model.

3 Discussion

We set out to meet the audacious goal of recovering a canonical algorithm only from neural data and sensory inputs. At first glance this seems impossible or at least ill-posed, but we showed that we could successfully recover structured latent message-passing dynamics in a distributed, multiplexed code, even when we don’t know the latent variables, structure, or algorithm in advance. We fit this model using time series of simulated neural activity and a set of external inputs, and a few assumptions about the underlying computation. Although these assumptions were significant, as described below, this work provides an important proof of concept for inferring inference, and subsequent studies can relax these assumptions for greater generality.

3.1 Related work

Past efforts to interpret neural activity have generally taken two complementary approaches: relating neural responses to task variables, or summarizing neural activity by low-dimensional latent variables. In the first case, task-relevant variables typically include sensory stimuli [55] and motor actions [56, 57, 58], but occasionally also include human-named latent variables like value or confidence [59, 60, 61, 62, 63, 64, 65, 66]. In contrast, dimensionality-reduction methods are often claimed to be interpretable simply due to their lower dimensionality compared to the full neural dimensionality [67, 68, 69]. Our work combines these two approaches by identifying representations of latent variables while also attributing meaning from their structured statistical interactions.

Given our foundational model assumptions, this combination led directly to a computationally constrained statistical neural data analysis [70, 71, 72, 73]. Other analysis methods share this aim of discovering latent computational functions from data, as opposed to a phenomenological description of the data. One prominent group of such studies includes inverse reinforcement learning [74, 75], inverse optimal control [76, 77, 78], and inverse rational control [66, 79, 80]. However, these approaches provide interpretability of behavioral data, not neural data as we use here. Some approaches attempt to jointly model behavior and neural data [70, 81], using the same latent variables for both. Perhaps the closest to our approach philosophically is [82], which aims to discover optimality principles of a neural network by analyzing neural activity.

Our approach to discovering computations is premised upon structured dynamics. Here we aim to discover inferential dynamics, but other approaches aim to discover a wide variety of other types of parsimonious interactions. Some of these use constrained nonlinear dynamics operating directly on observables, whereas others allow the dynamics to be hidden behind a subset of imperfect observations.

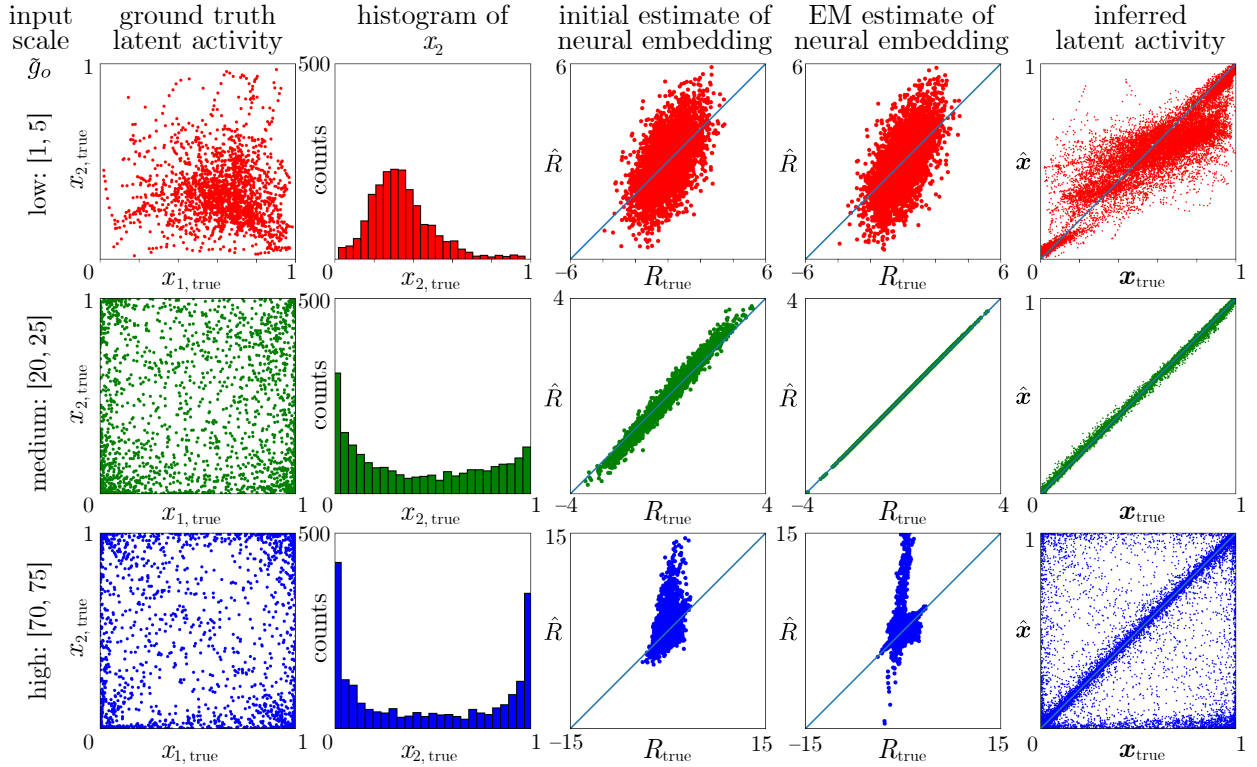


Figure 4: Importance of experiment design for inferring latent structure. Each row corresponds to a different range of amplitude scaling factor of the inputs \tilde{g}_o relative to the coupling strengths. The top, middle, and bottom rows correspond to low, medium, and high input gain ranges, respectively. The first column from the left shows a scatter plot of two components of the ground truth latent activity (x_1, x_2) of the example TAP brain in Fig. 3. The second column shows the histogram of one component of the ground truth latent activity (x_2). The third column from the left shows scatter plots of the initial ICA estimate of the neural embedding matrix vs. the ground truth. Similarly, the fourth column corresponds to the EM estimate of the neural embedding. The rightmost column shows a scatter plot of the inferred latent activity vs. the ground truth latent activity. When low-gain inputs (top row/red) are used, the latent dynamics are in a localized regime and the resulting ICA estimate \hat{R} is poor. This leads to degenerate solutions with Particle EM. On the other hand, when the input gain is too high (bottom row/blue), the latent activity is more biased towards maximal and minimal values. The resulting ICA estimate of the neural embedding \hat{R} has large deviations from the ground truth along multiple dimensions, again leading to suboptimal inference of the latent dynamics. However, when the input gain is the range [20, 25] (middle row/green), the latent dynamics exhibit a fairly uniform distribution of the latent states. In this regime, ICA is able to obtain a good initial estimate \hat{R} . With this initialization, Particle EM correctly estimates the neural encoding dimensions and the latent activity.

The past studies that concentrated on directly observable variables often have applications of inferring physical laws [29, 83, 84], biochemical reaction networks [85], neural connectivity [86], or interactions between more general objects [28]. These methods differ from ours because they identify structured interactions amongst predefined variables, whereas we also discover the latent variables themselves and their embedding in neural activity.

Other graph-based relational learning approaches aim to learn the latent variables, like our approach, but many localize the representation of each variable within a dedicated population [21, 27, 87, 88]. This approach has been used for learnable graph-based inference in probabilistic graphical models [34, 36, 89, 90] and for structured world models [91]. A crucial difference between our approach and these past models is that we allow structure to be multiplexed across population activity [13, 20, 92, 93].

Ample other work also aims to discover latent dynamics within neural activity or other observables. These use different assumptions about the linearity of the assumed dynamics and of the embedding. The most common approach is to model latent nonlinear dynamics as embedded linearly within observations. Our proposal falls into this category, although below we describe possible generalizations that relax this restriction. The most similar work to ours is perhaps [26],

who discover low-dimensional circuit structure within neural manifolds. Another example of this approach is switching linear dynamical systems, which approximate nonlinear dynamics by a piecewise linear dynamics [94, 95, 96, 97]. Other methods express observations as linear combinations of smooth functions for the nonlinear dynamics, via such mechanisms as recurrent neural networks [98, 99] or Gaussian processes [68, 100].

An alternative approach discovers linear dynamics within nonlinear embeddings. The Koopman operator [101] demonstrates that a sufficiently high-dimensional nonlinear embedding, such as a time-delay embedding [84, 102, 103], can transform nonlinear dynamics into linear dynamics, as used in some studies of motor control [104, 105, 106]. Fewer studies examine nonlinear dynamics in nonlinear embeddings, because these model are generally underconstrained. However, suitable regularization can provide enough structure to fruitfully fit nonlinear dynamics within curved data manifolds. For example, [107] uses sparse identification of nonlinear dynamics (SINDy) within a learned nonlinear embedding. While these latent variable dynamics can involve components with specific subsets of latent variables, previous approaches do not have inductive biases that favor graph-structured interactions with canonical functions. This additional structure in our approach may provide greater interpretability than these other more generic latent variable methods, and might help provide a better match to internal modeling of causality in the world that we and others hypothesize is a core element of cognition [14, 29, 88, 108].

Future work may find it fruitful to merge behavioral and latent algorithmic models using both behavioral and neural data. Such an approach could provide constraints on structured internal models that define distributed computations in behavioral tasks [70, 72], and could infer how computations are decoded to generate actions [109, 110, 111, 112].

3.2 Limitations and generalizations

Although our method of inferring inference discovers a surprising amount of structure, it still makes significant assumptions that would be good to relax in future incarnations.

Our foundational assumption is that the brain computes via canonical message-passing on graphs. This imposes an algorithmic symmetry that distinguishes *generic* nonlinear dynamics from *structured* nonlinear dynamics. In some sense this assumption is trivially true, if nodes are neurons and the graph is the anatomical connections between them. Notably, we did *not* assume that the computational graph corresponded to an anatomical connectivity graph in any way, although we could use such data from large-scale functional connectomics [113] to constrain our models [86]. However, just as in statistical physics, it may be that a simpler macroscopic picture emerges from the collective behavior of many microscopic elements [15, 114]. Ultimately it is an empirical question whether our hypothesis of canonical, low-dimensional message-passing computation parsimoniously describes brain computation [14, 3]. To evaluate this hypothesis on real data, it will be helpful to compare the performance of our model to that of other models described above, and even compare to relaxed versions of our own method without canonical (shared) message functions [115].

We also made model-specific assumptions that simplified this difficult inference problem. These can be grouped into assumptions about the brain’s internal model, the neural representation of that model, and the class of dynamics.

Assumptions about the brain’s internal model

Our strongest (and arguably worst) assumptions restricted the class of probabilistic graphical models being used for inference. In particular, our method assumed — correctly in this case — that the synthetic brain assumed that the latent world states were binary, so its beliefs were marginal probabilities. Technically, any generic graphical models can be approximated by a binary one [116], but this may require unduly complex interaction structures. It would often be more natural to consider richer classes of graphical models accounting for continuous variables [90, 117]. Additionally, here we only considered pairwise interactions, so our method would require some generalization to accommodate richer internal models that include multi-way interactions between variables [36, 118, 35]. Next, among pairwise graphical models, we considered only undirected, static models. It should be fairly straightforward to generalize our approach to accommodate directed acyclic graphs that can capture causal structure. This could include models with Markovian latent dynamics, allowing inferences to actually use sequences of observation (thus far we did allow sequences of observations, but the modeled inferences were static, with no temporal predictions for future observations). Finally, it may be beneficial to allow more flexibility than our shallow nonlinear polynomial message functions (Eq. 4), instead using neural networks to parameterize these message functions [27, 28, 34] which we may then analyze to find interpretable interaction patterns [90]. Such flexibility would introduce new global degeneracies that would allow compensating transformations of the interactions and message functions without changing the dynamics (this is a generalization of the compensating scaling we see between coupling energies and inference parameters, Figure S1). The complexity of these degeneracies could be reduced by regularizing the message function to depend smoothly on the interaction strengths.

Assumptions about the neural representation

The assumptions of binary latent variables and linear embeddings made it easier to identify the neural representation — particularly the manifold in which the dynamics operate — because marginal probabilities lie within a hypercube. When good experimental design exposes the full dynamic range of the inferred marginals, the bounded edges of this hypercube structure create a platykurtic distribution within neural activity that can be discovered by linear Independent Components Analysis, even without accounting for the dynamics. If the brain linearly represents the same marginals in a different manner, for example as log-probabilities, then we could in principle identify either a nonlinear embedding of the marginals [107, 119], or a linear embedding of the log-marginals [64]. Our work can be generalized to accommodate such nonlinear embeddings, although this will introduce additional degeneracies between the inferred embedding and inferred dynamics. For example, a message function that combines independent evidence can be expressed as products of probabilities, or sums of log-probabilities. Some of these degeneracies may be broken by assuming additional constraints on the nonlinear embeddings, while other degeneracies will remain [120].

Assumptions about dynamics

Our results showed that graphical model structure is a key property that reduces representational degeneracies. Even for flexible parametric or sampling-based representations of joint distributions, sparse graph-structured interactions between variables can provide a core computational constraint. Graph-structured interactions are a foundation of causal models as well, since graph assumptions are used to draw conclusions that go beyond the pure data [121].

While arbitrary graphs could in principle be paired with arbitrarily complex message functions like look-up tables to overfit observable data from a mismatched sparse graph, the erroneously inferred interactions will not generalize. Thus, to learn sparse graphs, we must constrain the message functions so they are not arbitrarily complex. Here we accomplished this by parameterizing the functions by a nonlinear basis (here, low-order polynomials) and penalizing their coefficients [122]. More general parameterizations, as in a graph neural network [27, 28, 29], might need to be regularized to favor smoothness, or could exploit implicit biases to allow smooth functions to emerge automatically [123, 124].

An alternative approach to modeling dynamics is to use an embedding space that is sufficiently high dimensional that all nonlinear dynamics in the original space can be expressed as linear dynamics in the embedding space [101, 103, 104]. Although some of the graph structure could be preserved as block-structured linear dynamics, such a method would use a higher-dimensional state space that would make interpretation much more difficult.

Even though our model of the brain does include dynamics, those are only inference dynamics, in a world that is assumed to be static. While we do allow the external evidence to change over time, the current underlying inference model treats these as noisy or mismatched observations rather than reflections of a changing world state. Subsequent versions of inferring inference should address this limitation by allowing an internal model based on a *spatiotemporal* graph: a directed, time-translation-invariant Markov chain with internal spatial structure. This is a natural format for graph-structured causal variables describing a dynamic world. This could arise from a hierarchical model of activity, and/or by continually learning interactions. Our framework could be augmented to account for these effects, including possibly inferring plasticity rules [125].

Here we assumed the brain used essentially deterministic message-passing dynamics, although we allowed some small non-computational process noise. Alternative inference theories, notably sampling-based codes [43, 30, 126, 127, 32], use randomness for a computational function. Local sampling approaches, like Gibbs sampling, can be seen as stochastic message-passing, and our framework can be expanded to accommodate these dynamics as well. One interesting hybrid is to perform a temporal dimensionality reduction on the stochastic dynamics, smoothing time series while computing time-dependent nonlinear statistics at the fast timescale (*e.g.* slowly changing means and variances) that then flow through the graph via deterministic message-passing [14].

3.3 Outlook

To apply our framework to real data, we will need responses of many neurons responding to the same stimuli, and we will need a significant duration of data. To capture the message-passing dynamics, it may be important to record by fast techniques like electrophysiology, because slower techniques like calcium imaging could blur away the relevant computations. While the computations estimated on this slow timescale may still be nonlinear, they may hide message-passing dynamics that best explain these nonlinearities.

Depending on the properties of the code and our modeling assumptions, it may be important to have simultaneously recorded neurons. For example, in a sampling-based code, the joint uncertainty is reflected by response covariations

[43, 127, 32]. Although these can be re-interpreted as nonlinear rate codes [65, 112] through expectation values [33], estimating these nonlinear statistics still requires simultaneous measurements.

The notion of a canonical operation is, in a deep sense, core to *any* form of understanding: one rule that explains multiple computations; an *explanans* that is simpler than the *explanandum*. For other theories of brain computation, this core explanation might be a plasticity rule, a goal and optimization method [128, 129], and/or prewired structure [7, 130, 131].

How could the brain implement a canonical operation? Unlike machine learning algorithms, it is unable to copy synaptic weights to multiple locations during learning. We see three possibilities: hardwiring, convergent learning, and modularity. Hardwired local microcircuits [132] and control structures are conserved across animals, and these may arise from genetically encoded developmental programs selected by evolution [7, 133]. Convergent learning could happen if a genetically encoded plasticity rule rediscovers a common algorithm multiple times across a graph because that is the optimal solution for many problems [134]. In between these extremes, it may be that system-wide architecture imposes bottlenecks that create a modular architecture [22, 135, 136, 137], so this module’s computations can be ‘copied over time’ by applying it sequentially to differently inputs gated through the module. Our analysis approach could discover canonical computations, regardless of mechanism.

Although quite flexible, message-passing computation on graphs is not universal. It cannot, for example, distinguish between graphs and their covers (larger graphs that pass over the original nodes multiple times) [138, 139]. The class of message-passing algorithms could potentially predict specific inferential errors, like overcounting evidence — predictions that we could directly test with suitably designed behavioral and neural experiments.

Modern neuroscience is acquiring massive amounts of data, such as the MICrONS project [113] and the Allen Brain Observatory [140], providing new opportunities to understand brain function. To make sense of these massive datasets, we need principled mathematical frameworks [14, 66, 82, 73, 141, 142]. The current approach of *inferring inference* may provide a novel way of identifying graph structure and canonical operations that the brain uses to model its environment and guide its actions.

4 Methods

4.1 Constructing a model brain that performs approximate inference

4.1.1 Model inference dynamics

We use TAP dynamics as a model of approximate inference. These dynamics follow the discrete-time update equations

$$x_{it+1} = (1 - \lambda)x_{it} + \lambda \sigma \left(\sum_{j=1}^{N_s} \mathcal{M}(x_{it}, x_{jt}, J_{ij}) + (V\mathbf{o}_t)_i \right) + \xi_{it} \quad i = 1, \dots, N_s \quad (5)$$

where $\lambda \in (0, 1]$ is a relaxation parameter that sets a timescale for the dynamics, $\sigma(z) = 1/(1 + e^{-z})$ is a sigmoid function that affects the update operation (Eq. 3), the aggregation function is a sum (Eq. 2), and \mathcal{M} is the canonical message function (Eq. 1) shared across the graphical model. The TAP message function has the specific polynomial form,

$$\mathcal{M}(x_i, x_j, J_{ij}) = 2J_{ij}x_j + 4J_{ij}^2(1 - 2x_i)x_j(1 - x_j) \quad (6)$$

Unlike the usual TAP equation, we also add a small amount of Gaussian process noise ξ_t to emulate the stochasticity found in brains’ real dynamics and allow for some model mismatch.

4.1.2 Constructing a model brain

The model brain is a two-layer recurrent neural network (RNN):

$$\mathbf{r}_{t+1}^{\text{hid}} = \text{ReLU} \left(W_{\text{rec}}^{\text{hid}} \mathbf{r}_t^{\text{hid}} + W_{\text{ff}}^{\text{hid}} \mathbf{o}_t + \mathbf{b}^{\text{hid}} \right) \quad (7)$$

$$\mathbf{r}_{t+1} = \text{ReLU} \left(W_{\text{rec}} \mathbf{r}_t + W_{\text{ff}} \mathbf{r}_t^{\text{hid}} + \mathbf{b} \right) \quad (8)$$

where $\text{ReLU}(x) = \max(0, x)$ is the Rectified Linear Unit activation function, \mathbf{o}_t is the input to the network, and $\mathbf{r}_t^{\text{hid}}$ and \mathbf{r}_t are the activities of the hidden and output layers, respectively. $\{W_{\text{rec}}^{\text{hid}}, W_{\text{rec}}\}$, $\{W_{\text{ff}}^{\text{hid}}, W_{\text{ff}}\}$ and $\{\mathbf{b}^{\text{hid}}, \mathbf{b}\}$ are the recurrent, feed-forward weights and biases of the RNN. This network is trained so the activity of the output layer is an approximate linear embedding of TAP dynamics on an underlying graphical model (eq. 5).

The network has N_h hidden layer neurons and N_r output neurons. For our simulation example, we constructed a model brain with $N_r = 500$ output neurons, $N_h = 1000$ hidden layer neurons, and inputs of dimension $N_o = 10$. We chose this two-layer recurrent architecture because it was much easier to reproduce the desired latent dynamics than a single layer recurrent network. In all of our experiments with inferring inference for TAP model brains, we observe only the activity of the second layer neurons \mathbf{r}_t .

To construct this network, we must choose the coupling matrix that defines the assumed graphical model J , input mapping matrix V , and the neural embedding matrix R . For the coupling matrix J , we generated a $N_s \times N_s$ sparse, symmetric adjacency matrix with sparsity of 0.5. The non-zero elements of the coupling matrix were then sampled from $\mathcal{N}(0, 1.5)$. For the input mapping matrix V , we used an orthogonal matrix obtained from the singular vectors in the singular value decomposition of a random $N_s \times N_o$ matrix with entries sampled independently from $\mathcal{N}(0, 1)$. The elements of the $N_r \times N_s$ neural embedding matrix R were also sampled independently from $\mathcal{N}(0, 1.5)$.

For the chosen set of parameters and the time series of inputs \mathbf{o}_t described below, we generate the corresponding TAP dynamics \mathbf{x}_t using Equation 5, providing a target, $R\mathbf{x}_t + \mathbf{b}$, for training the RNN. The constant bias vector \mathbf{b} is chosen to ensure that the target neural activity in the output layer is always positive. We train the network to minimize the squared error between the output neural activity and the target: $\sum_t \|\mathbf{r}_t - R\mathbf{x}_t - \mathbf{b}\|_2^2$. For computing the MSE, we ignored the first $T_{\text{clip}} = 20$ time-steps of the RNN activity for each batch. We optimize the weights and biases of the RNN using the Adam optimizer[143] with a learning rate of 10^{-5} , mini-batch size of 16, and 8×10^5 training iterations.

4.1.3 Input signal design

The choice of the input signals \mathbf{o}_t was crucial both for training the TAP model brain and indeed for applying the inferring inference analysis framework.

The inference algorithm enacted by the TAP equation assumes inputs are constant, and the dynamics in equation 5 converge to a fixed point. To get more data about the underlying algorithm, we use dynamic input signals, contrary to the model brain's inference algorithm's assumptions. We chose these dynamic inputs to be filtered versions of random piecewise constant functions \tilde{o}_t held constant for T_{const} time-steps. At the start of each period, each input variable \tilde{o}_i ($i = 1, \dots, N_o$) is generated independently as $\tilde{o}_i = \gamma_i \nu_i$, where $\nu_i \sim \mathcal{N}(0, 1)$. The amplitude scaling term is drawn from a Gamma distribution $\gamma_i \sim \Gamma(\kappa, g_o)$, where $\kappa = 1$ is the shape parameter, $g_o = \tilde{g}_o / \sqrt{N_s}$ is the scale parameter, and N_s is the number of latent variables in the TAP model brain. We then pass the raw input sequence \tilde{o}_t through a forward-backward filter to obtain \mathbf{o}_t . This is done to smoothen transitions between successive time periods. A normalized Hamming window of length N_{Ham} is used as the impulse response of the filter. For each batch we sampled integer T_{const} from the discrete uniform distribution $\mathcal{U}[2, 5]$. We set $N_{\text{Ham}} = 5$ as the Hamming window length for the temporal smoothing filter.

When training the model brain, we used $\tilde{g}_o \sim \mathcal{U}[2, 50]$ for the continuous amplitude scaling distribution. We generated input signals for training the model brain with the following settings. We used $B_{\text{train}} = 25000$ training batches, each of length $T = 50$ time-steps. When inferring the algorithm of this model brain, we instead varied the amplitude as described in Figure 4.

4.2 Inferring model parameters from simulated data

4.2.1 Maximizing model likelihood

In this section we describe the Particle EM algorithm used to obtain the maximum likelihood estimate of the TAP brain parameters. The goal is to compute the maximum likelihood estimate of $\boldsymbol{\theta}$,

$$\hat{\boldsymbol{\theta}} = \underset{\boldsymbol{\theta}}{\text{argmax}} \, p(\mathbf{r}_{0:T} | \mathbf{o}_{0:T}; \boldsymbol{\theta}) = \underset{\boldsymbol{\theta}}{\text{argmax}} \, \int p(\mathbf{x}_{0:T}, \mathbf{r}_{0:T} | \mathbf{o}_{0:T}; \boldsymbol{\theta}) d\mathbf{x}_{0:T}. \quad (9)$$

The joint distribution of the latent and observed neural activity given the inputs is given by the Hidden Markov Model

$$p(\mathbf{x}_{0:T}, \mathbf{r}_{0:T} | \mathbf{o}_{0:T}; \boldsymbol{\theta}) = p(\mathbf{x}_0) \prod_{t=0}^{T-1} p(\mathbf{x}_{t+1} | \mathbf{x}_t, \mathbf{o}_t; \boldsymbol{\theta}) \prod_{t=0}^T p(\mathbf{r}_t | \mathbf{x}_t; \boldsymbol{\theta}), \quad (10)$$

where $\boldsymbol{\theta} = (R, V, J, G)$ are the parameters to be estimated. The transition density and the conditional marginal density are specified as:

$$p(\mathbf{x}_{t+1} | \mathbf{x}_t, \mathbf{o}_t; \boldsymbol{\theta}) = \mathcal{N}(\boldsymbol{\mu}(\mathbf{x}_t, \mathbf{o}_t; \boldsymbol{\theta}), \boldsymbol{\Sigma}_\xi) \quad (11a)$$

$$p(\mathbf{r}_t | \mathbf{x}_t; \boldsymbol{\theta}) = \mathcal{N}(R\mathbf{x}_t, \boldsymbol{\Sigma}_\eta) \quad (11b)$$

where Σ_ξ, Σ_η are the covariances of the process noise and measurement noise, respectively. The conditional mean of the transition probability is obtained by using the general polynomial form of the message function in Equation 5,

$$\mu_i(\mathbf{x}_t, \mathbf{o}_t; \boldsymbol{\theta}) = (1 - \lambda)x_{it} + \lambda \sigma \left(\sum_{j,a,b,c} G_{abc} J_{ij}^a x_{it}^b x_{jt}^c + (V \mathbf{o}_t)_i \right). \quad (12)$$

A standard approach for computing maximum likelihood estimates of unknown parameters in models involving latent variables is the EM algorithm [49]. However, the E-step requires us to compute the expected value of the complete data log likelihood with respect to the posterior distribution of the latent variables given the current estimate of the parameters $\boldsymbol{\theta}_n$,

$$Q(\boldsymbol{\theta}, \boldsymbol{\theta}_n) \triangleq \mathbb{E}_{\boldsymbol{\theta}_n} [\log p(\mathbf{x}_{0:T}, \mathbf{r}_{0:T} | \mathbf{o}_{0:T}; \boldsymbol{\theta})]. \quad (13)$$

We use a particle filter to approximate the posterior distribution required in the E-step, and we use gradient ascent to perform the M-step (Supplementary Section S1).

4.2.2 Greedy optimization of the message-passing parameters

We observe two broad classes of degeneracies in our optimization. The first class involves the neural embedding. We can recover latent dynamics that are just a linear transformation away from the true latent variable dynamics, $\hat{\mathbf{x}}_t \approx A\mathbf{x}_t$, in a way that is exactly compensated by a change in the neural embedding, $\hat{R} = RA$ (Fig. S1A). The second class of degeneracies involves both the coupling parameters J and the canonical message-parameters G . Here, we recover the correct latent representations and dynamics, yet the estimates \hat{J} and \hat{G} differ from the ground truth. One simple version is that we can scale all the coupling terms J_{ij} globally by any factor β , and then perfectly compensate by scaling the each message-passing coefficient G_{abc} by β^{-a} . This is equivalent to increasing the interaction energies and inference ‘temperature’ at the same time, and leads to identical latent dynamics. Fig. S1B–D illustrates a typical degeneracy of this type.

To quantify the full range of degeneracies locally, we compute the curvature matrix (Hessian) of the mean squared prediction error at the ground-truth parameters, and compute the eigenvalues and eigenvectors of this Hessian (Fig. S1E,F). Eigenvectors with small eigenvalues indicate directions of low curvature, where prediction quality is similar as the model parameters change. Fig. S1 shows several directions with small eigenvalues of the curvature matrix, revealing that there are several other interesting degeneracies between the interactions J and message parameters G , all of which give rise to very similar latent dynamics.

Inferring the true latent representations and dynamics requires us to break these degeneracies in the parameterization. One potential approach is to use prior knowledge about the brain’s internal model and introduce the appropriate inductive biases in our optimization framework. For instance, to break the degeneracy in the neural embedding, we might assume the latent states of the model brain are bounded from above and below, consistent with our assumed sigmoidal update function \mathcal{U} . This favors using Independent Component Analysis [144] to initialize the estimated neural embedding matrix \hat{R} , since it is effective at discovering embeddings of platykurtic distributions.

To break the degeneracies in estimates of the coupling matrix \hat{J} and the message-passing parameters \hat{G} obtained from Particle EM, we find the smallest subset of \hat{G} that best fits the inferred latent dynamics. This can be formulated as a minimization problem with ℓ_0 regularization, adding an ℓ_0 -regularization term $\|G\|_0$ to the loss. General ℓ_0 optimization is combinatorially hard, so we adopt a backward greedy approximation to find parameters that best explain the latent dynamics. In this approach, we begin with the full set of polynomial terms in equation 4 used during Particle EM, and successively eliminate the least significant polynomial term G_{abc} until the regularized loss stops decreasing.

4.2.3 Inferring an example TAP brain

For inferring inference in the example TAP brain described in the previous section, we first generated 2000 and 25000 batches of data for the ICA and Particle EM steps, respectively. Each batch of neural activity was generated using inputs with $T = 25$ time-steps, input correlation time $T_{\text{const}} \sim \mathcal{U}[2, 5]$, and amplitude scaling factor $\tilde{g}_0 \sim \mathcal{U}[5, 25]$.

For each assumed value of \hat{N}_s , we perform ICA to obtain an initial estimate of \hat{R} . We also initialize the bias term \hat{b} to the mean of the neural activity across all batches and neurons. We initialize the remaining parameters as follow. The canonical message parameters \hat{G} were sampled from $\mathcal{N}(0, 0.01)$. For the coupling matrix \hat{J} , we generated a dense, symmetric matrix whose elements were sampled from $\mathcal{N}(0, 0.05)$. For the input mapping matrix \hat{V} , we used an orthogonal matrix that was obtained from the singular value decomposition of a matrix of size $N_s \times N_o$ with entries sampled from $\mathcal{N}(0, 1)$.

For the Particle EM step, we assume that the process noise has a small variance of 10^{-5} . We also assume prior knowledge of the covariance of the measurement noise. For the amplitude scaling factor settings used to generate our inputs, we set the covariance of the measurement noise to a diagonal matrix with variance of 0.08 for each neuron. Note that we can also estimate this covariance using neural activity from the TAP brain when the input is held constant for a long duration and the TAP dynamics converge to fixed points for constant inputs. We run Particle EM for 25000 iterations, using 4 batches of data per iteration. The 4 batches are selected randomly from the 25000 batches of data at the start of each iteration. For the particle filter, we use $K = 100$ particles. For the M-step we use the Adam optimizer with a learning rate of 2×10^{-3} . We lower this learning rate to 1×10^{-3} and 5×10^{-4} after 12500 and 18750 iterations, respectively. To evaluate the Particle EM estimates, we use $B_{\text{test}} = 500$ batches of test data generated using the aforementioned input settings.

Next, we use the parameters corresponding to the optimal \hat{N}_s , to run the particle filter on 2000 batches of test data (also generated using the same input settings previously described). We used the latent activity obtained from this particle filter to run the greedy backward optimization step to refine the estimates of the coupling matrix and the canonical message parameters. We exclude the terms that are quadratic in both x_{it} and x_{jt} while initializing the greedy search. These terms contribute to one of the dominant degeneracies in our parameterization (see eigenvector 2 in Fig. S1F). For each subset of \hat{G} parameters, we minimize the ℓ_0 -regularized loss function using the Adam optimizer with a learning rate of 10^{-2} , mini-batch size of 100, and 4000 iterations. We use $\gamma = 2 \times 10^{-6}$ as the weighting factor for the ℓ_0 regularization.

4.3 Code

Code reproducing these results can be found at <https://github.com/XaqLab/InferringInference/>.

4.4 Acknowledgments

The authors thank Andreas Tolias, Krešimir Josić, and Rich Zemel for helpful conversations.

This work was supported in part NSF CAREER grant 1552868 and the Intelligence Advanced Research Projects Activity (IARPA) via Department of Interior/Interior Business Center (DoI/IBC) contract number D16PC00003. The U.S. Government is authorized to reproduce and distribute reprints for Governmental purposes notwithstanding any copyright annotation thereon. Disclaimer: the views and conclusions contained herein are those of the authors and should not be interpreted as necessarily representing the official policies or endorsements, either expressed or implied, of IARPA, DoI/IBC, or the U.S. Government.

4.5 Declaration of interests

XP is a co-founder of Upload AI, LLC.

References

- [1] Kenneth D Miller. Canonical computations of cerebral cortex. *Current opinion in neurobiology*, 37:75–84, 2016.
- [2] Matteo Carandini and David J Heeger. Normalization as a canonical neural computation. *Nature Reviews Neuroscience*, 13(1):51–62, 2012.
- [3] Gary Marcus, Adam Marblestone, and Tom Dean. The atoms of neural computation. *Science*, 346:551–552, 2014. Computational Neuroscience.
- [4] David Marr et al. Vision: A computational investigation into the human representation and processing of visual information, 1982.
- [5] Roger C Conant and W Ross Ashby. Every good regulator of a system must be a model of that system. *International journal of systems science*, 1(2):89–97, 1970.
- [6] David H Wolpert and William G Macready. No free lunch theorems for optimization. *IEEE transactions on evolutionary computation*, 1(1):67–82, 1997.
- [7] Anthony M Zador. A critique of pure learning and what artificial neural networks can learn from animal brains. *Nature communications*, 10(1):1–7, 2019.
- [8] Anirudh Goyal and Yoshua Bengio. Inductive biases for deep learning of higher-level cognition. *Proceedings of the Royal Society A*, 478(2266):20210068, 2022.

[9] H Helmholtz. *Treatise on physiological optics. volume iii. the perceptions of vision; trans. into english by optical society of america.* menasha, wisconsin, 1925.

[10] Kenji Doya. *Bayesian brain: Probabilistic approaches to neural coding.* MIT press, 2007.

[11] Daphne Koller and Nir Friedman. *Probabilistic graphical models: principles and techniques.* MIT press, 2009.

[12] Rajkumar Vasudeva Raju and Xaq Pitkow. Marginalization in random nonlinear neural networks. In *APS March Meeting Abstracts*, volume 1, page 1107p, 2015.

[13] Rajkumar Vasudeva Raju and Xaq Pitkow. Inference by reparameterization in neural population codes. In *Advances in Neural Information Processing Systems*, pages 2029–2037, 2016.

[14] Xaq Pitkow and Dora E Angelaki. Inference in the brain: statistics flowing in redundant population codes. *Neuron*, 94(5):943–953, 2017.

[15] Shreya Saxena and John P Cunningham. Towards the neural population doctrine. *Current opinion in neurobiology*, 55:103–111, 2019.

[16] R Becket Ebitz and Benjamin Y Hayden. The population doctrine in cognitive neuroscience. *Neuron*, 109(19):3055–3068, 2021.

[17] Matthew R Whiteway and Daniel A Butts. The quest for interpretable models of neural population activity. *Current Opinion in Neurobiology*, 58:86–93, 2019.

[18] Rafael Yuste. From the neuron doctrine to neural networks. *Nature reviews neuroscience*, 16(8):487–497, 2015.

[19] Apostolos P Georgopoulos, Andrew B Schwartz, and Ronald E Kettner. Neuronal population coding of movement direction. *Science*, 233(4771):1416–1419, 1986.

[20] Mattia Rigotti, Omri Barak, Melissa R Warden, Xiao-Jing Wang, Nathaniel D Daw, Earl K Miller, and Stefano Fusi. The importance of mixed selectivity in complex cognitive tasks. *Nature*, 497(7451):585–590, 2013.

[21] Sara Sabour, Nicholas Frosst, and Geoffrey E Hinton. Dynamic routing between capsules. *arXiv preprint arXiv:1710.09829*, 2017.

[22] Zack Dulberg, Rachit Dubey, Isabel M Berwian, and Jonathan D Cohen. Modularity benefits reinforcement learning agents with competing homeostatic drives. *arXiv preprint arXiv:2204.06608*, 2022.

[23] Semir M Zeki. Functional organization of a visual area in the posterior bank of the superior temporal sulcus of the rhesus monkey. *The Journal of physiology*, 236(3):549–573, 1974.

[24] Daniel J Felleman and David C Van Essen. Distributed hierarchical processing in the primate cerebral cortex. *Cerebral cortex (New York, NY: 1991)*, 1(1):1–47, 1991.

[25] Simon Musall, Matthew T Kaufman, Ashley L Juavinett, Steven Gluf, and Anne K Churchland. Single-trial neural dynamics are dominated by richly varied movements. *bioRxiv*, page 308288, 2019.

[26] Christopher Langdon and Tatiana A Engel. Latent circuit inference from heterogeneous neural responses during cognitive tasks. *bioRxiv*, pages 2022–01, 2022.

[27] Franco Scarselli, Marco Gori, Ah Chung Tsoi, Markus Hagenbuchner, and Gabriele Monfardini. The graph neural network model. *IEEE Transactions on Neural Networks*, 20(1):61–80, 2009.

[28] Thomas Kipf, Ethan Fetaya, Kuan-Chieh Wang, Max Welling, and Richard Zemel. Neural relational inference for interacting systems. *arXiv preprint arXiv:1802.04687*, 2018.

[29] Peter W Battaglia, Jessica B Hamrick, Victor Bapst, Alvaro Sanchez-Gonzalez, Vinicius Zambaldi, Mateusz Malinowski, Andrea Tacchetti, David Raposo, Adam Santoro, Ryan Faulkner, et al. Relational inductive biases, deep learning, and graph networks. *arXiv preprint arXiv:1806.01261*, 2018.

[30] Tai Sing Lee and David Mumford. Hierarchical bayesian inference in the visual cortex. *JOSA A*, 20(7):1434–1448, 2003.

[31] Iris Vilares and Konrad Kording. Bayesian models: the structure of the world, uncertainty, behavior, and the brain. *Annals of the New York Academy of Sciences*, 1224(1):22–39, 2011.

[32] Ralf M Haefner, Pietro Berkes, and József Fiser. Perceptual decision-making as probabilistic inference by neural sampling. *Neuron*, 90(3):649–660, 2016.

[33] Eszter Vértes and Maneesh Sahani. Flexible and accurate inference and learning for deep generative models. In *Advances in Neural Information Processing Systems*, pages 4166–4175, 2018.

[34] KiJung Yoon, Renjie Liao, Yuwen Xiong, Lisa Zhang, Ethan Fetaya, Raquel Urtasun, Richard Zemel, and Xaq Pitkow. Inference in probabilistic graphical models by graph neural networks. *arXiv preprint arXiv:1803.07710*, 2018.

[35] Zhen Zhang, Fan Wu, and Wee Sun Lee. Factor graph neural networks. *Advances in Neural Information Processing Systems*, 33:8577–8587, 2020.

[36] Yicheng Fei and Xaq Pitkow. Generalization of graph network inferences in higher-order probabilistic graphical models. *arXiv preprint arXiv:2107.05729*, 2021.

[37] Manfred Opper and David Saad. *Advanced mean field methods: Theory and practice*. MIT press, 2001.

[38] Judea Pearl. *Probabilistic reasoning in intelligent systems: networks of plausible inference*. Morgan Kaufmann, 1988.

[39] Thomas P Minka. Expectation propagation for approximate bayesian inference. In *Proceedings of the Seventeenth conference on Uncertainty in artificial intelligence*, pages 362–369. Morgan Kaufmann Publishers Inc., 2001.

[40] Rubén Moreno-Bote, Jeffrey Beck, Ingmar Kanitscheider, Xaq Pitkow, Peter Latham, and Alexandre Pouget. Information-limiting correlations. *Nature Neuroscience*, 17:1410–1417, 2014.

[41] Cristina Savin and Sophie Deneve. Spatio-temporal representations of uncertainty in spiking neural networks. In *Advances in Neural Information Processing Systems*, pages 2024–2032, 2014.

[42] Sophie Deneve. Bayesian spiking neurons i: inference. *Neural computation*, 20(1):91–117, 2008.

[43] Patrik O Hoyer and Aapo Hyvärinen. Interpreting neural response variability as monte carlo sampling of the posterior. In *Advances in neural information processing systems*, pages 293–300, 2003.

[44] Richard D Lange, Ari S Benjamin, Ralf M Haefner, and Xaq Pitkow. Interpolating between sampling and variational inference with infinite stochastic mixtures. In *Uncertainty in Artificial Intelligence*, pages 1063–1073. PMLR, 2022.

[45] David J Thouless, Philip W Anderson, and Robert G Palmer. Solution of ‘solvable model of a spin glass’. *Philosophical Magazine*, 35(3):593–601, 1977.

[46] Manfred Opper and Ole Winther. Tractable approximations for probabilistic models: The adaptive thouless-anderson-palmer mean field approach. *Physical Review Letters*, 86(17):3695, 2001.

[47] Tatsuto Murayama. Thouless-anderson-palmer approach for lossy compression. *Physical Review E*, 69(3):035105, 2004.

[48] Maoz Shamir and Haim Sompolinsky. Thouless-anderson-palmer equations for neural networks. *Physical Review E*, 61(2):1839, 2000.

[49] Arthur P Dempster, Nan M Laird, and Donald B Rubin. Maximum likelihood from incomplete data via the em algorithm. *Journal of the Royal Statistical Society: Series B (Methodological)*, 39(1):1–22, 1977.

[50] Olivier Cappé, Simon J Godsill, and Eric Moulines. An overview of existing methods and recent advances in sequential monte carlo. *Proceedings of the IEEE*, 95(5):899–924, 2007.

[51] Nikolas Kantas, Arnaud Doucet, Sumeetpal S Singh, Jan Maciejowski, Nicolas Chopin, et al. On particle methods for parameter estimation in state-space models. *Statistical science*, 30(3):328–351, 2015.

[52] Peiran Gao, Eric Trautmann, Byron Yu, Gopal Santhanam, Stephen Ryu, Krishna Shenoy, and Surya Ganguli. A theory of multineuronal dimensionality, dynamics and measurement. *BioRxiv*, page 214262, 2017.

[53] Mikhail Genkin and Tatiana A Engel. Moving beyond generalization to accurate interpretation of flexible models. *Nature machine intelligence*, 2(11):674–683, 2020.

[54] Aapo Hyvärinen and Erkki Oja. Independent component analysis: algorithms and applications. *Neural networks*, 13(4-5):411–430, 2000.

[55] David H Hubel and Torsten N Wiesel. Receptive fields, binocular interaction and functional architecture in the cat’s visual cortex. *The Journal of physiology*, 160(1):106–154, 1962.

[56] Mark M Churchland, John P Cunningham, Matthew T Kaufman, Justin D Foster, Paul Nuyujukian, Stephen I Ryu, and Krishna V Shenoy. Neural population dynamics during reaching. *Nature*, 487(7405):51, 2012.

[57] Ryan C Williamson, Brent Doiron, Matthew A Smith, and M Yu Byron. Bridging large-scale neuronal recordings and large-scale network models using dimensionality reduction. *Current opinion in neurobiology*, 55:40–47, 2019.

[58] John P Cunningham and M Yu Byron. Dimensionality reduction for large-scale neural recordings. *Nature neuroscience*, 17(11):1500, 2014.

[59] Jan Gläscher, Nathaniel Daw, Peter Dayan, and John P O’Doherty. States versus rewards: dissociable neural prediction error signals underlying model-based and model-free reinforcement learning. *Neuron*, 66(4):585–595, 2010.

[60] Nathaniel D Daw, Yael Niv, and Peter Dayan. Uncertainty-based competition between prefrontal and dorsolateral striatal systems for behavioral control. *Nature neuroscience*, 8(12):1704–1711, 2005.

[61] J Yu Angela and Peter Dayan. Uncertainty, neuromodulation, and attention. *Neuron*, 46(4):681–692, 2005.

[62] Clara Kwon Starkweather, Benedicte M Babayan, Naoshige Uchida, and Samuel J Gershman. Dopamine reward prediction errors reflect hidden-state inference across time. *Nature neuroscience*, 20(4):581–589, 2017.

[63] Wei Ji Ma, Jeffrey M Beck, Peter E Latham, and Alexandre Pouget. Bayesian inference with probabilistic population codes. *Nature neuroscience*, 9(11):1432–1438, 2006.

[64] Edgar Y Walker, R James Cotton, Wei Ji Ma, and Andreas S Tolias. A neural basis of probabilistic computation in visual cortex. *Nature Neuroscience*, 23(1):122–129, 2020.

[65] Olivier J Hénaff, Zoe M Boundy-Singer, Kristof Meding, Corey M Ziembra, and Robbe LT Goris. Representation of visual uncertainty through neural gain variability. *Nature communications*, 11(1):1–12, 2020.

[66] Zhengwei Wu, Minhae Kwon, Saurabh Daptardar, Paul Schrater, and Xaq Pitkow. Rational thoughts in neural codes. *Proceedings of the National Academy of Sciences*, 117(47):29311–29320, 2020.

[67] Joshua Glaser, Matthew Whiteway, John P Cunningham, Liam Paninski, and Scott Linderman. Recurrent switching dynamical systems models for multiple interacting neural populations. *Advances in neural information processing systems*, 33:14867–14878, 2020.

[68] Lea Duncker, Gergo Bohner, Julien Boussard, and Maneesh Sahani. Learning interpretable continuous-time models of latent stochastic dynamical systems. In *International Conference on Machine Learning*, pages 1726–1734. PMLR, 2019.

[69] Qiang Huang, Makoto Yamada, Yuan Tian, Dinesh Singh, Dawei Yin, and Yi Chang. Graphlime: Local interpretable model explanations for graph neural networks. *arXiv preprint arXiv:2001.06216*, 2020.

[70] Brandon M Turner, Birte U Forstmann, Eric-Jan Wagenmakers, Scott D Brown, Per B Sederberg, and Mark Steyvers. A bayesian framework for simultaneously modeling neural and behavioral data. *NeuroImage*, 72:193–206, 2013.

[71] Daniel Durstewitz, Georgia Koppe, and Hazem Toutounji. Computational models as statistical tools. *Current Opinion in Behavioral Sciences*, 11:93–99, 2016.

[72] Scott W Linderman and Samuel J Gershman. Using computational theory to constrain statistical models of neural data. *Current opinion in neurobiology*, 46:14–24, 2017.

[73] Wiktor Mlynarski, Michal Hledík, Thomas R Sokolowski, and Gašper Tkačík. Statistical analysis and optimality of neural systems. *Neuron*, 109(7):1227–1241, 2021.

[74] Andrew Y Ng, Stuart J Russell, et al. Algorithms for inverse reinforcement learning. In *ICML*, volume 1, page 2, 2000.

[75] Monica Babes, Vukosi Marivate, Kaushik Subramanian, and Michael L Littman. Apprenticeship learning about multiple intentions. In *Proceedings of the 28th International Conference on Machine Learning (ICML-11)*, pages 897–904, 2011.

[76] Krishnamurthy Dvijotham and Emanuel Todorov. Inverse optimal control with linearly-solvable mdps. In *ICML*, 2010.

[77] Felix Schmitt, Hans-Joachim Bieg, Michael Herman, and Constantin A Rothkopf. I see what you see: Inferring sensor and policy models of human real-world motor behavior. In *Aaai*, pages 3797–3803, 2017.

[78] Dominik Straub and Constantin A Rothkopf. Putting perception into action: Inverse optimal control for continuous psychophysics. *bioRxiv*, 2021.

[79] Minhae Kwon, Saurabh Daptardar, Paul Schrater, and Xaq Pitkow. Inverse rational control with partially observable continuous nonlinear dynamics. *Advances in Neural Information Processing Systems*, in press.

[80] Daniel Jarrett, Alihan Hüyük, and Mihaela Van Der Schaar. Inverse decision modeling: Learning interpretable representations of behavior. In *International Conference on Machine Learning*, pages 4755–4771. PMLR, 2021.

[81] Brandon M Turner, Birte U Forstmann, Bradley C Love, Thomas J Palmeri, and Leendert Van Maanen. Approaches to analysis in model-based cognitive neuroscience. *Journal of Mathematical Psychology*, 76:65–79, 2017.

[82] Matthew Chalk, Gasper Tkacik, and Olivier Marre. Inferring the function performed by a recurrent neural network. *Plos one*, 16(4):e0248940, 2021.

[83] Michael Schmidt and Hod Lipson. Distilling free-form natural laws from experimental data. *science*, 324(5923):81–85, 2009.

[84] Peter J Baddoo, Benjamin Herrmann, Beverley J McKeon, J Nathan Kutz, and Steven L Brunton. Physics-informed dynamic mode decomposition (pidmd). *arXiv preprint arXiv:2112.04307*, 2021.

[85] Yuki Shindo, Yohei Kondo, and Yasushi Sako. Inferring a nonlinear biochemical network model from a heterogeneous single-cell time course data. *Scientific reports*, 8(1):1–10, 2018.

[86] Lu Mi, Richard Xu, Sridhama Prakhy, Albert Lin, Nir Shavit, Aravinthan Samuel, and Srinivas C Turaga. Connectome-constrained latent variable model of whole-brain neural activity. In *International Conference on Learning Representations*, 2021.

[87] Edgar Xi, Selina Bing, and Yang Jin. Capsule network performance on complex data. *arXiv preprint arXiv:1712.03480*, 2017.

[88] Anirudh Goyal, Alex Lamb, Jordan Hoffmann, Shagun Sodhani, Sergey Levine, Yoshua Bengio, and Bernhard Schölkopf. Recurrent independent mechanisms. *arXiv preprint arXiv:1909.10893*, 2019.

[89] Meng Qu, Yoshua Bengio, and Jian Tang. GMNN: Graph Markov neural networks. In Kamalika Chaudhuri and Ruslan Salakhutdinov, editors, *Proceedings of the 36th International Conference on Machine Learning*, volume 97 of *Proceedings of Machine Learning Research*, pages 5241–5250. PMLR, 09–15 Jun 2019.

[90] Zhe Li, Andreas S. Tolias, and Xaq Pitkow. Learning dynamics and structure of complex systems using graph neural networks, 2022.

[91] Thomas Kipf, Elise van der Pol, and Max Welling. Contrastive learning of structured world models. In *International Conference on Learning Representations*, 2019.

[92] Valerio Mante, David Sussillo, Krishna V Shenoy, and William T Newsome. Context-dependent computation by recurrent dynamics in prefrontal cortex. *nature*, 503(7474):78, 2013.

[93] Niru Maheswaranathan, Alex Williams, Matthew Golub, Surya Ganguli, and David Sussillo. Universality and individuality in neural dynamics across large populations of recurrent networks. *Advances in neural information processing systems*, 32, 2019.

[94] Zoubin Ghahramani and Geoffrey E Hinton. Variational learning for switching state-space models. *Neural computation*, 12(4):831–864, 2000.

[95] Emily Fox, Erik Sudderth, Michael Jordan, and Alan Willsky. Nonparametric bayesian learning of switching linear dynamical systems. *Advances in neural information processing systems*, 21, 2008.

[96] Scott Linderman, Matthew Johnson, Andrew Miller, Ryan Adams, David Blei, and Liam Paninski. Bayesian learning and inference in recurrent switching linear dynamical systems. In *Artificial Intelligence and Statistics*, pages 914–922, 2017.

[97] Aram Giahi Saravani, Kiefer Forseth, Nitin Tandon, and Xaq Pitkow. Dynamic brain interactions during visual naming. *Technical Report, Baylor College of Medicine*, 2018.

[98] Herbert Jaeger and Harald Haas. Harnessing nonlinearity: Predicting chaotic systems and saving energy in wireless communication. *Science*, 304(5667):78–80, 2004.

[99] Chethan Pandarinath, Daniel J O’Shea, Jasmine Collins, Rafal Jozefowicz, Sergey D Stavisky, Jonathan C Kao, Eric M Trautmann, Matthew T Kaufman, Stephen I Ryu, Leigh R Hochberg, et al. Inferring single-trial neural population dynamics using sequential auto-encoders. *Nature methods*, page 1, 2018.

[100] Jack Wang, Aaron Hertzmann, and David J Fleet. Gaussian process dynamical models. *Advances in neural information processing systems*, 18, 2005.

[101] Bernard O Koopman. Hamiltonian systems and transformation in hilbert space. *Proceedings of the National Academy of Sciences of the United States of America*, 17(5):315, 1931.

[102] Floris Takens. Detecting strange attractors in turbulence. In *Dynamical systems and turbulence, Warwick 1980*, pages 366–381. Springer, 1981.

[103] Peter J Schmid. Dynamic mode decomposition of numerical and experimental data. *Journal of fluid mechanics*, 656:5–28, 2010.

[104] Yuanjun Gao, Evan W Archer, Liam Paninski, and John P Cunningham. Linear dynamical neural population models through nonlinear embeddings. In *Advances in neural information processing systems*, pages 163–171, 2016.

[105] Daniel Bruder, C. David Remy, and Ram Vasudevan. Nonlinear system identification of soft robot dynamics using koopman operator theory. In *2019 International Conference on Robotics and Automation (ICRA)*, pages 6244–6250, 2019.

[106] Ian Abraham and Todd D Murphey. Active learning of dynamics for data-driven control using koopman operators. *IEEE Transactions on Robotics*, 35(5):1071–1083, 2019.

[107] Joseph Bakarji, Kathleen Champion, J Nathan Kutz, and Steven L Brunton. Discovering governing equations from partial measurements with deep delay autoencoders. *arXiv preprint arXiv:2201.05136*, 2022.

[108] Judea Pearl and Dana Mackenzie. *The book of why: the new science of cause and effect*. Basic books, 2018.

[109] Ralf M Haefner, Sebastian Gerwinn, Jakob H Macke, and Matthias Bethge. Inferring decoding strategies from choice probabilities in the presence of correlated variability. *Nature Neuroscience*, 16(2):235–242, 2013.

[110] Xaq Pitkow, Sheng Liu, Dora E Angelaki, Gregory C DeAngelis, and Alexandre Pouget. How can single sensory neurons predict behavior? *Neuron*, 87(2):411–423, 2015.

[111] Bruce G Cumming and Hendrikje Nienborg. Feedforward and feedback sources of choice probability in neural population responses. *Current opinion in neurobiology*, 37:126–132, 2016.

[112] Qianli Yang, Edgar Y Walker, R James Cotton, Andreas Savas Tolias, and Xaq S Pitkow. Revealing nonlinear neural decoding by analyzing choices. *Nature Communications*, page 332353, in press 2021.

[113] MICrONS Consortium. Functional connectomics spanning multiple areas of mouse visual cortex. *bioRxiv*, 2021.

[114] Erik P Hoel, Larissa Albantakis, and Giulio Tononi. Quantifying causal emergence shows that macro can beat micro. *Proceedings of the National Academy of Sciences*, 110(49):19790–19795, 2013.

[115] Steven L Brunton, Joshua L Proctor, and J Nathan Kutz. Discovering governing equations from data by sparse identification of nonlinear dynamical systems. *Proceedings of the National Academy of Sciences*, 113(15):3932–3937, 2016.

[116] T. Jebara. *Tractability: Practical Approaches to Hard Problems*, chapter Perfect graphs and graphical modeling. Cambridge Press, 2014.

[117] Kanti V Mardia, Gareth Hughes, Charles C Taylor, and Harshinder Singh. A multivariate von mises distribution with applications to bioinformatics. *Canadian Journal of Statistics*, 36(1):99–109, 2008.

[118] Frank R Kschischang, Brendan J Frey, and H-A Loeliger. Factor graphs and the sum-product algorithm. *IEEE Transactions on information theory*, 47(2):498–519, 2001.

[119] E Archer, IM Park, L Buesing, J Cunningham, and L Paninski. Black box variational inference for state space models. *arXiv*, stat.ML:1511.07367, 2015.

[120] Aapo Hyvärinen and Petteri Pajunen. Nonlinear independent component analysis: Existence and uniqueness results. *Neural networks*, 12(3):429–439, 1999.

[121] Judea Pearl. *Causality*. Cambridge university press, 2009.

[122] Steven L Brunton, Joshua L Proctor, and J Nathan Kutz. Sparse identification of nonlinear dynamics with control (sindyc). *arXiv preprint arXiv:1605.06682*, 2016.

[123] Francis Williams, Matthew Trager, Daniele Panozzo, Claudio Silva, Denis Zorin, and Joan Bruna. Gradient dynamics of shallow univariate relu networks. *Advances in neural information processing systems*, 32, 2019.

[124] Justin Sahs, Ryan Pyle, Aneel Damaraju, Josue Ortega Caro, Onur Tavaslioglu, Andy Lu, and Ankit Patel. Shallow univariate relu networks as splines: initialization, loss surface, hessian, & gradient flow dynamics. *arXiv preprint arXiv:2008.01772*, 2020.

[125] Sukbin Lim, Jillian L McKee, Luke Woloszyn, Yali Amit, David J Freedman, David L Sheinberg, and Nicolas Brunel. Inferring learning rules from distributions of firing rates in cortical neurons. *Nature neuroscience*, 18(12):1804–1810, 2015.

[126] David H Ackley, Geoffrey E Hinton, and Terrence J Sejnowski. A learning algorithm for boltzmann machines*. *Cognitive science*, 9(1):147–169, 1985.

[127] P. Berkes, G. Orban, M. Lengyel, and J. Fiser. Spontaneous cortical activity reveals hallmarks of an optimal internal model of the environment. *Science*, 331(6013):83–7, 2011.

[128] Blake A Richards, Timothy P Lillicrap, Philippe Beaudoin, Yoshua Bengio, Rafal Bogacz, Amelia Christensen, Claudia Clopath, Rui Ponte Costa, Archy de Berker, Surya Ganguli, Colleen J. Gillon, Danijar Hafner, Adam Kepecs, Nikolaus Kriegeskorte, Peter Latham, Grace W Lindsay, Kenneth D Miller, Richard Naud, Christopher C Pack, Panayiota Poirazi, Pieter Roelfsema, João Sacramento, Andrew Saxe, Benjamin Scellier, Anna C Schapiro,

Walter Senn, Greg Wayne, Daniel Yamins, Friedemann Zenke, Joel Zylberberg, Denis Therien, and Konrad P Kording. A deep learning framework for neuroscience. *Nature neuroscience*, 22(11):1761–1770, 2019.

[129] Charles Darwin. *On the origin of species*, 1859. Routledge, 2004.

[130] Wolfgang Maass, Thomas Natschläger, and Henry Markram. Real-time computing without stable states: A new framework for neural computation based on perturbations. *Neural computation*, 14(11):2531–2560, 2002.

[131] Fabian H Sinz, Xaq Pitkow, Jacob Reimer, Matthias Bethge, and Andreas S Tolias. Engineering a less artificial intelligence. *Neuron*, 103(6):967–979, 2019.

[132] Vernon B Mountcastle. Central nervous mechanisms in mechanoreceptive sensibility. *Comprehensive Physiology*, pages 789–878, 2011.

[133] Paul Cisek. Resynthesizing behavior through phylogenetic refinement. *Attention, Perception, & Psychophysics*, 81(7):2265–2287, 2019.

[134] A Emin Orhan and Wei Ji Ma. Efficient probabilistic inference in generic neural networks trained with non-probabilistic feedback. *Nature communications*, 8(1):1–14, 2017.

[135] Laureline Logiaco, LF Abbott, and Sean Escola. Thalamic control of cortical dynamics in a model of flexible motor sequencing. *Cell reports*, 35(9):109090, 2021.

[136] Sebastian Musslick and Jonathan D Cohen. Rationalizing constraints on the capacity for cognitive control. *Trends in Cognitive Sciences*, 25(9):757–775, 2021.

[137] Ruiyi Zhang, Xaq Pitkow, and Dora E Angelaki. Inductive biases of neural networks for generalization in spatial navigation. *bioRxiv*, pages 2022–12, 2022.

[138] Zhengdao Chen, Soledad Villar, Lei Chen, and Joan Bruna. On the equivalence between graph isomorphism testing and function approximation with gnns. *Advances in neural information processing systems*, 32, 2019.

[139] Ryoma Sato. A survey on the expressive power of graph neural networks. *arXiv preprint arXiv:2003.04078*, 2020.

[140] Saskia EJ de Vries, Jerome A Lecoq, Michael A Buice, Peter A Groblewski, Gabriel K Ocker, Michael Oliver, David Feng, Nicholas Cain, Peter Ledochowitsch, Daniel Millman, et al. A large-scale standardized physiological survey reveals functional organization of the mouse visual cortex. *Nature Neuroscience*, 23(1):138–151, 2020.

[141] Karl Friston. The free-energy principle: a unified brain theory? *Nature reviews neuroscience*, 11(2):127–138, 2010.

[142] Yi Ma, Doris Tsao, and Heung-Yeung Shum. On the principles of parsimony and self-consistency for the emergence of intelligence. *arXiv preprint arXiv:2207.04630*, 2022.

[143] Diederik P Kingma and Jimmy Ba. Adam: A method for stochastic optimization. *arXiv preprint arXiv:1412.6980*, 2014.

[144] Pierre Comon. Independent component analysis, a new concept? *Signal processing*, 36(3):287–314, 1994.

[145] Tiancheng Li, Miodrag Bolic, and Petar M Djuric. Resampling methods for particle filtering: classification, implementation, and strategies. *IEEE Signal processing magazine*, 32(3):70–86, 2015.

[146] Arnaud Doucet and Adam M Johansen. A tutorial on particle filtering and smoothing: Fifteen years later. *Handbook of nonlinear filtering*, 12(656-704):3, 2009.

[147] Geoffrey McLachlan and Thriyambakam Krishnan. *The EM algorithm and extensions*, volume 382. John Wiley & Sons, 2007.

S1 Particle Expectation Maximization

A particle filter approximates the posterior over the latent variables given the current estimate of the model parameters as

$$\hat{p}(\mathbf{x}_{0:T} | \mathbf{r}_{0:T}; \hat{\boldsymbol{\theta}}_n) = \sum_{k=1}^K w^{(k)} \delta(\mathbf{x}_{0:T} - \mathbf{x}_{0:T}^{(k)}) \quad (14)$$

where δ is the Dirac delta function. The samples $\{\mathbf{x}_{0:T}^{(k)}\}_{k=1}^K$ are referred to as particles. Each particle represents one hypothesis about the state of the system, and the corresponding importance weight $w^{(k)}$ is a measure of how

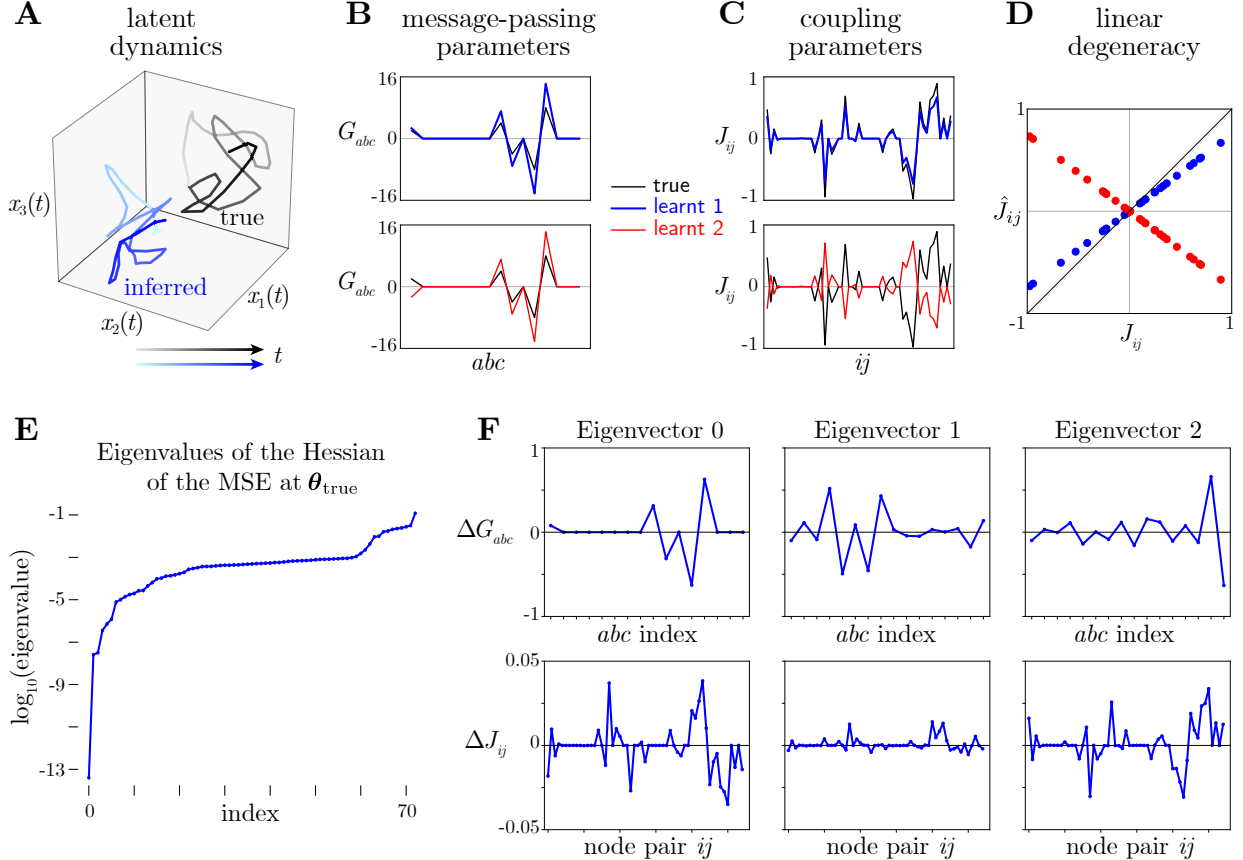


Figure S1: **Degeneracies in our parameterization.** **A:** Latent states decoded by a particle filter (blue) versus true latent states (black). This visualization shows that the decoded trajectory is a linear transformation of the true trajectory. **B,C:** If we fix the embedding to the correct value, and relearn the remaining parameters twice, then the two sets of parameters (red, blue) both provide reasonable matches to the message-passing parameters and couplings of the true model (black). Couplings \hat{J}_{ij} (estimates) and J_{ij} (true) are related by a linear transformation for each of the two solutions, shown in panel **D**. \hat{J}_{ij} in panel **C** and the corresponding message-passing parameters \hat{G} in panel **B** result in an inference algorithm that is equivalent to the true model. **E:** Log-eigenvalues of the curvature (Hessian) of the mean squared prediction error for the latent dynamics at the true parameter values. Small values indicate degeneracies. **F:** The G and J components (top and bottom rows, respectively) of the eigenvectors corresponding to the three smallest eigenvalues. Parameter perturbations along eigenvector 0 correspond to the linear degeneracy between the interactions and the message passing parameters seen in **B–D**.

probable that particular latent trajectory is. To sample the particle trajectories, we use the following sequential sampling distribution:

$$\begin{aligned} q(\mathbf{x}_t | \mathbf{x}_{t-1}, \mathbf{r}_t) &= p(\mathbf{x}_t | \mathbf{x}_{t-1}, \mathbf{r}_t; \boldsymbol{\theta}_n) \\ &= \frac{p(\mathbf{x}_t | \mathbf{x}_{t-1}; \boldsymbol{\theta}_n) p(\mathbf{r}_t | \mathbf{x}_t; \boldsymbol{\theta}_n)}{p(\mathbf{r}_t | \mathbf{x}_{t-1}; \boldsymbol{\theta}_n)} \end{aligned} \quad (15)$$

The unnormalized weight for each particle can also be sequentially updated as

$$\tilde{w}_t^{(k)} \propto \tilde{w}_{t-1}^{(k)} p(\mathbf{r}_t | \mathbf{x}_{t-1}^{(k)}; \boldsymbol{\theta}_n) \quad (16)$$

Since the conditional distributions in Equations 11a, b are Gaussian, we can analytically derive the sequential sampling distribution and corresponding weight update as:

$$p(\mathbf{x}_t | \mathbf{x}_{t-1}, \mathbf{r}_t; \boldsymbol{\theta}_n) = \mathcal{N}(P_n^{-1} \mathbf{v}_t, P_n^{-1}) \quad (17a)$$

$$p(\mathbf{r}_t | \mathbf{x}_{t-1}; \boldsymbol{\theta}_n) = \kappa \exp \left\{ -\frac{1}{2} \left(\boldsymbol{\mu}_{t-1}^\top \Sigma_\xi^{-1} \boldsymbol{\mu}_{t-1} + \mathbf{r}_t^\top \Sigma_\eta^{-1} \mathbf{r}_t - \mathbf{v}_t^\top P_n \mathbf{v}_t \right) \right\} \quad (17b)$$

where

$$P_n = \Sigma_\xi^{-1} + R_n^\top \Sigma_\eta^{-1} R_n \quad (18a)$$

$$\mathbf{v}_t = \Sigma_\xi^{-1} \boldsymbol{\mu}_{t-1} + R_n^\top \Sigma_\eta^{-1} \mathbf{r}_t \quad (18b)$$

R_n is the current estimate of the neural embedding matrix, and κ is a normalization constant. The conditional mean $\boldsymbol{\mu}_{t-1}$ is obtained using equation 12 with the current estimates of the input mapping matrix V_n , coupling matrix J_n , message parameters G_n , and inputs \mathbf{o}_{t-1} .

Algorithm 1: Particle filter

Initialization;

Given current estimates of parameters $\boldsymbol{\theta}_n$,

Sample $\mathbf{x}_0^{(k)} \sim \mathcal{N}(R_n^\dagger \mathbf{r}_1, \Sigma_\xi)$, assign initial weight $w_0^{(k)} = \frac{1}{K}$, for $k = 1, \dots, K$

Set observed data likelihood $\mathcal{L}_0 = 1$

for $t = 1$ to T **do**

 Propagate the trajectories:

for $k = 1$ to K **do**

 Sample $\mathbf{x}_t^{(k)} \sim \mathcal{N}(P_n^{-1} \mathbf{v}_t^{(k)}, P_n^{-1})$

 Update weight, $\tilde{w}_t^{(k)} = w_{t-1}^{(k)} p(\mathbf{r}_t | \mathbf{x}_{t-1}^{(k)}; \boldsymbol{\theta}_n)$

end

 Update the likelihood: $\mathcal{L}_t = \mathcal{L}_{t-1} \times \left(\sum_{k=1}^K \tilde{w}_t^{(k)} \right)$

 Normalize the weights: $w_t^{(k)} = \frac{\tilde{w}_t^{(k)}}{\sum_{j=1}^K \tilde{w}_t^{(j)}}, k = 1, \dots, K$

if $\hat{K}_{\text{eff}} < K/2$ **then**

 ResampleSystematic $\left\{ w_t^{(k)}, \mathbf{x}_{0:t}^{(k)} \right\}_{k=1}^K$

end

end

In practice, the importance weights tend to become degenerate after a few time steps, in the sense that most of the samples have very small weights and thus do not significantly contribute to the approximation of the target distribution. This sample impoverishment problem is circumvented using resampling. If the effective sample size

$$\hat{K}_{\text{eff}} \triangleq \frac{1}{\sum_{k=1}^K \left(w_t^{(k)} \right)^2} \quad (19)$$

falls below a chosen threshold, the current population of particles are resampled using normalized weights as probabilities of selection. Trajectories with small weights are eliminated, and those with large importance weights are replicated. After resampling, the importance weights are reset to $1/K$. There are several ways of performing resampling; the systematic resampling algorithm [145] is used here.

An important property of the particle filter is that the observed data likelihood can also be updated sequentially as a function of the unnormalized weights \tilde{w} [146],

$$\hat{p}(\mathbf{r}_{0:t}) = \prod_{\tau=0}^t \left\{ \sum_{k=1}^K \tilde{w}_\tau^{(k)} \right\} \quad (20)$$

Algorithm 1 presents all the steps of the particle filter used in our analysis of the TAP brain models. In each iteration of EM, the approximation to the posterior in terms of the particles can be used to simplify the E-step (equation 13) as:

$$\begin{aligned} Q(\boldsymbol{\theta}, \boldsymbol{\theta}_n) &= \sum_{k=1}^K w_T^{(k)} \log p(\mathbf{x}_{0:T}^{(k)}, \mathbf{r}_{0:T} | \mathbf{o}_{0:T}; \boldsymbol{\theta}) \\ &= \sum_{k=1}^K w_T^{(k)} \left\{ \log p(\mathbf{x}_0^{(k)}) + \sum_{t=1}^T \log p(\mathbf{x}_t^{(k)} | \mathbf{x}_{t-1}^{(k)}, \mathbf{o}_{t-1}; \boldsymbol{\theta}) + \log p(\mathbf{r}_t | \mathbf{x}_t^{(k)}; \boldsymbol{\theta}) \right\} \end{aligned} \quad (21)$$

Ignoring all the constant terms, this can be further simplified as,

$$Q(\boldsymbol{\theta}, \boldsymbol{\theta}_n) = -\frac{1}{2} \sum_{k=1}^K w_T^{(k)} \sum_{t=1}^T \left\{ \left(\mathbf{x}_t^{(k)} - \boldsymbol{\mu}_{t-1}^{(k)} \right)^\top \Sigma_\xi^{-1} \left(\mathbf{x}_t^{(k)} - \boldsymbol{\mu}_{t-1}^{(k)} \right) + \left(\mathbf{r}_t - R\mathbf{x}_t^{(k)} \right)^\top \Sigma_\eta^{-1} \left(\mathbf{r}_t - R\mathbf{x}_t^{(k)} \right) \right\} \quad (22)$$

where the conditional mean $\boldsymbol{\mu}_{t-1}^{(k)} = \boldsymbol{\mu}_{t-1}^{(k)}(\mathbf{x}_{t-1}^{(k)}, \mathbf{o}_{t-1}; \boldsymbol{\theta})$ is obtained from equation 12.

The Q function derived in the E-step is non-convex because the conditional mean is a nonlinear function of the parameters $\boldsymbol{\theta}$. Thus, a closed form solution for the maximum is not available. Instead, on each M-step, we perform one iteration of gradient ascent on $Q(\boldsymbol{\theta}, \boldsymbol{\theta}_n)$ using the Adam optimizer [143]. This optimization does not find the maximum value of $Q(\boldsymbol{\theta}, \boldsymbol{\theta}_n)$. However, the updated parameters $\boldsymbol{\theta}_{n+1}$ satisfy,

$$Q(\boldsymbol{\theta}_{n+1}, \boldsymbol{\theta}_n) \geq Q(\boldsymbol{\theta}_n, \boldsymbol{\theta}_n). \quad (23)$$

This approach, to simply increase and not necessarily maximize $Q(\boldsymbol{\theta}, \boldsymbol{\theta}_n)$, is known as the Generalized Expectation Maximization (GEM) algorithm and is useful in cases like ours where the maximization in the M-step is difficult [147].

The Particle EM algorithm used in the analysis of the TAP brain is summarized in algorithm 2.

Algorithm 2: Particle EM

Initialize parameters $\boldsymbol{\theta}_0$;

while observed data likelihood has not converged **do**

- 1. Use particle filter (algorithm 1) to obtain $\hat{p}(\mathbf{x}_{0:T} | \mathbf{r}_{0:T}, \mathbf{o}_{0:T}; \boldsymbol{\theta}_n)$
- 2. E step: use particles $\{\mathbf{x}_{0:T}^{(k)}\}_{k=1}^K$ to compute $Q(\boldsymbol{\theta}, \boldsymbol{\theta}_n)$
- 3. M step: obtain $\boldsymbol{\theta}_{n+1}$ using one iteration of Adam optimizer on $Q(\boldsymbol{\theta}, \boldsymbol{\theta}_n)$

end
